J. Fluid Mech. (2010), *vol.* 657, *pp.* 36–63.
doi:10.1017/S0022112010001345

A variational approach to Boussinesq modelling of fully nonlinear water waves

GERT KLOPMAN[1]†, BRENNY VAN GROESEN[1] AND MAARTEN W. DINGEMANS[2]

[1]Applied Analysis and Mathematical Physics, University of Twente, PO Box 217, 7500 AE Enschede, The Netherlands

[2]Delft Hydraulics, Boomkensdiep 11, 8303 KW Emmeloord, The Netherlands

(Received 19 July 2009; revised 10 March 2010; accepted 10 March 2010)

In this paper we present a new method to derive Boussinesq-type equations from a variational principle. These equations are valid for nonlinear surface-water waves propagating over bathymetry. The vertical structure of the flow, required in the Hamiltonian, is approximated by a (series of) vertical shape functions associated with unknown parameter(s). It is not necessary to make approximations with respect to the nonlinearity of the waves. The resulting approximate Hamiltonian is positive definite, contributing to the good dynamical behaviour of the resulting equations. The resulting flow equations consist of temporal equations for the surface elevation and potential, as well as a (set of) elliptic equations for some auxiliary parameter(s). All equations only contain low-order spatial derivatives and no mixed time–space derivatives. Since one of the parameters, the surface potential, can be associated with a uniform shape function, the resulting equations are very well suited for wave–current interacting flows.

The variational method is applied to two simple models, one with a parabolic vertical shape function and the other with a hyperbolic-cosine vertical structure. For both, as well as the general series model, the flow equations are derived. Linear dispersion and shoaling are studied using the average Lagrangian. The model with a parabolic vertical shape function has improved frequency dispersion, as compared to classical Boussinesq models. The model with a hyperbolic-cosine vertical structure can be made to have exact phase and group velocity, as well as shoaling, for a certain frequency.

For the model with a parabolic vertical structure, numerical computations are done with a one-dimensional pseudo-spectral code. These show the nonlinear capabilities for periodic waves over a horizontal bed and an underwater bar. Further some long-distance computations for soliton wave groups over bathymetry are presented.

1. Introduction

The discovery of the Hamilton theory for surface-water waves, independently made by Zakharov (1968), Broer (1974) and Miles (1977) (see also Milder 1977), was associated with the search for approximate Hamiltonian models containing as much as possible of the essential characteristics of the exact theory. While Zakharov (1968)

† Email address for correspondence: G.Klopman@math.utwente.nl

focused especially on deep-water waves, Broer (1974, 1975) and Miles (1977) also paid attention to relatively long waves of Boussinesq type.

Positive definiteness of the Hamiltonian is one of the important properties of the Hamiltonian, since it contributes to the good dynamical behaviour of the resulting equations. Non-positivity of the approximate Hamiltonian may lead to instabilities (see e.g. Milder 1990; Broer 1974; Katopodes & Dingemans 1989).

Dingemans (1997, § 5.6) describes several methods for constructing Boussinesq-type models with positive-definite Hamiltonian, but these methods are quite tedious and have certain ambiguities regarding the order of certain operators (see also Broer 1974, 1975; Broer, van Groesen & Timmers 1976). The described models are weakly nonlinear.

Further, there is the demand for improved frequency dispersion and nonlinear characteristics in Boussinesq models, as compared to the classical ones. As a result, several improved Boussinesq-type models have been developed, starting with Madsen, Murray & Sørensen (1991) and Madsen & Sørensen (1992) using methods of Witting (1984). Another step was made with the introduction of a high-order nonlinear Boussinesq-type model in Agnon, Madsen & Schäffer (1999) (see also Madsen, Bingham & Schäffer 2003; Fuhrman & Bingham 2004), which uses the free-surface boundary conditions as found from Hamilton theory. However, the additional approximations to relate the free-surface quantities to those at another fixed level destroy the positive definiteness of the Hamiltonian. The same is true for other high-order methods (e.g. Dommermuth & Yue 1987; West *et al.* 1987).

Lynett & Liu (2004*a*,*b*) derive a (non-Hamiltonian) Boussinesq-type of model in which they use a multi-layer approach in the vertical. In each layer they use a parabolic vertical structure for the horizontal velocity, and a linear one for the vertical velocity. By adding layers, the frequency-dispersion characteristics can be improved (Lynett & Liu 2004*b*; Hsiao *et al.* 2005).

A fully nonlinear and positive-definite Hamiltonian model for waves over bathymetry has been devised by Radder (1992), which however is of quite complicated form especially when constructing numerical solutions (Otta, Dingemans & Radder 1996). See Radder (1999) for a review of Hamiltonian models for water waves.

Here, we will present a variational method to derive Boussinesq models for water waves over bathymetry (for shortness, we will call these variational Boussinesq models). The present method is relatively easy, leads to a positive-definite Hamiltonian and can be fully nonlinear if desired. Besides the general form we also give some simple examples for three different vertical velocity-potential structures: parabolic, hyperbolic cosine and from a power series. We restrict ourselves to mildly sloping bathymetry, to simplify the resulting equations, but this is not essential to the method. The advantage of the present variational Boussinesq model is that no higher-order spatial and/or mixed spatial-temporal derivatives appear. But, this is at the cost of the requirement to solve one or more additional linear elliptic equations in the horizontal plane.

First, we will outline the methodology of our method in § 2. Then, in § 3, we will apply this to a simple parabolic shape function. Thereafter we will present the general case of a series of vertical shape functions and associated parameters in § 4. Also two more examples of the method will be given, one with a cosh (hyperbolic-cosine) vertical shape function, and another with a power-series representation of the vertical structure. Some linear characteristics, e.g. frequency dispersion and shoaling by depth changes, will be studied in § 5. For this we will use the average Lagrangian technique of Whitham (1974), and apply it also to the three model examples. Finally, in § 6, we will present numerical simulations using the parabolic vertical-structure model, in

order to study the applicability and nonlinear characteristics of the model. Periodic waves and confined wave groups will be computed, both when propagating over a horizontal bed, as well as over bathymetry.

2. Variational principle and modelling

We start from the variational principle for irrotational surface-water waves on an incompressible inviscid homogeneous fluid, in the form as given by Miles (1977). With $\phi(\boldsymbol{x}, z, t)$ the velocity potential, $\zeta(\boldsymbol{x}, t)$ the free-surface elevation and $\varphi(\boldsymbol{x}, t) \equiv \phi(\boldsymbol{x}, \zeta(\boldsymbol{x}, t), t)$ the velocity potential at the free surface, we have

$$0 = \delta \mathscr{L} = \delta \iint\!\!\!\int L \, \mathrm{d}\boldsymbol{x} \, \mathrm{d}t \tag{2.1a}$$

with

$$L = \varphi \partial_t \zeta - H \quad \text{and} \quad H = \int_{-h_0}^{\zeta} \frac{1}{2} \left[(\nabla\phi)^2 + (\partial_z \phi)^2 \right] \mathrm{d}z + \frac{1}{2} g \zeta^2. \tag{2.1b}$$

Here $\mathscr{L}(\zeta, \varphi)$ is the Lagrangian, $L(\zeta, \varphi; \boldsymbol{x}, t)$ is the associated Lagrangian density per unit of horizontal area and time and $H(\zeta, \varphi; \boldsymbol{x}, t)$ is the Hamiltonian density, i.e. the sum of the kinetic and potential energy densities per unit area. The horizontal and vertical coordinates are $\boldsymbol{x} = (x_1, x_2)^T$ and z, respectively, and t is the time coordinate. The irrotational fluid flow is described by a velocity potential $\phi(\boldsymbol{x}, z, t)$, with the horizontal and vertical flow velocities given by $\nabla\phi$ and $\partial_z\phi$, respectively, where $\nabla \equiv (\partial_{x_1}, \partial_{x_2})^T$ is the horizontal gradient operator. Term $(\nabla\phi)^2$ denotes the inner product $(\nabla\phi)\cdot(\nabla\phi)$. The fluid domain is bounded below by the sea bed at $z = -h_0(\boldsymbol{x})$ and above by a free surface at $z = \zeta(\boldsymbol{x}, t)$. Further, g is the acceleration due to gravity, the fluid mass density is taken to be constant and equal to 1.

As shown by Miles (1977), the above Lagrangian variational principle is equivalent to the Hamiltonian approach. The Hamiltonian $\mathscr{H}(\zeta, \varphi; t)$ itself is the spatial integral of (2.1*b*):

$$\mathscr{H} = \iint H \, \mathrm{d}\boldsymbol{x}. \tag{2.2}$$

The flow dynamics are completely described by ζ and φ, provided that in the fluid interior the Laplace equation is satisfied, as well as the kinematic boundary condition at the seabed (Zakharov 1968; Broer 1974; Milder 1977; Miles 1977).

While the above equations are exact and give all the equations necessary for the description of the flow, they are in general not solvable in closed form. Therefore, for practical applications approximations have to be made. We directly model the horizontal and vertical velocities, $\nabla\phi$ and $\partial_z\phi$, in the Hamiltonian density H, equation (2.1*b*), and apply this in the variational principle (2.1*a*). In doing so, several characteristics of the exact Hamiltonian system can be transferred into the approximate flow equations. By Noether's theorem, symmetries in the variational principle translate into conservation laws (see e.g. Benjamin & Olver 1982; Benjamin 1984; Brizard 2005). Among these are conservation of energy and mass; this is due to the independence of the Hamiltonian of time translations and of the choice of the zero level of the velocity potential. In general, the Hamiltonian is not constant under changes of the horizontal position $\boldsymbol{x}$, since the still water depth h_0 is a function of $\boldsymbol{x}$. So, apart from the special case when h_0 is a constant, horizontal momentum will not be conserved. But conservation of mass and energy can easily be maintained in approximate models (as well as horizontal momentum for the case of h_0 constant). Another property of the Hamiltonian density (2.1*b*) is that it is positive definite.

For shortness of notation, the summation convention is used throughout this paper, i.e. a repeated index that indicates summation is used:

$$\alpha_m \beta_m \equiv \sum_{m=1}^{M} \alpha_m \beta_m. \tag{2.3}$$

Repeated italic indices indicate summation from 1 to M.

Since we are interested in large horizontal domains with the surface waves propagating horizontally, we choose to approximate the potential ϕ in the fluid interior by a vertical structure:

$$\phi(\boldsymbol{x}, z, t) = \varphi(\boldsymbol{x}, t) + f_m(z; h_0, \zeta, \kappa_m)\psi_m(\boldsymbol{x}, t) \tag{2.4a}$$

with

$$f_m = 0 \quad \text{at } z = \zeta(\boldsymbol{x}, t) \tag{2.4b}$$

for $m = 1, 2 \ldots M$. Here $f_m(z; h_0, \zeta, \kappa_m)$ are the prescribed vertical shape functions associated with the parameters $\psi_m(\boldsymbol{x}, t)$ for $m = 1, 2 \ldots M$, with M the (small) number of shape functions used. Further, the $\kappa_m(\boldsymbol{x})$ are optional shape parameters, which may eventually be specified (e.g. an expected curvature of the velocity profile based on knowledge of the incoming wave field). Note that we assume $\kappa_m(\boldsymbol{x})$ to be known and fixed *a priori*.

The requirement (2.4*b*) is essential: the shape functions f_m have to be zero at the free surface. It guarantees that only two evolution equations with simple time derivatives $\partial_t \zeta$ and $\partial_t \varphi$ will appear, when taking the variational derivatives with respect to the surface potential φ and elevation ζ of the term $\varphi \partial_t \zeta$ in the Lagrangian (2.1). Notice that Whitham (1967), in deriving Boussinesq-type equations using a Lagrangian variational approach, also remarks that the flow equations become simpler in terms of the surface potential. In the approximation (2.4*a*), the first term $\varphi(\boldsymbol{x}, t)$ can be thought of as being associated with a uniform shape function, i.e. equal to 1 for all z. This means that the model will always include a description well suited to interactions between short waves and long waves or currents. As a result, we have the following Hamiltonian description in terms of the canonical variables ζ and φ:

$$\partial_t \zeta = +\frac{\delta \mathscr{H}}{\delta \varphi} \qquad \text{and} \qquad \partial_t \varphi = -\frac{\delta \mathscr{H}}{\delta \zeta} \tag{2.5a}$$

under the requirement that

$$\frac{\delta \mathscr{H}}{\delta \psi_m} = 0 \qquad \text{for } m = 1, 2 \ldots M, \tag{2.5b}$$

where $\delta \mathscr{H}/\delta \zeta$, $\delta \mathscr{H}/\delta \varphi$ and $\delta \mathscr{H}/\delta \psi_m$ denote the variational derivatives of $\mathscr{H}(\zeta, \varphi, \psi_m)$ with respect to ζ, φ and ψ_m, respectively.

Using (2.4*a*), we have the following expressions for the flow velocities:

$$\nabla\phi = \nabla\varphi + f_m \nabla\psi_m + (\partial_\zeta f_m)\psi_m \nabla\zeta + (\partial_{h_0} f_m)\psi_m \nabla h_0 + (\partial_{\kappa_m} f_m)\psi_m \nabla\kappa_m, \tag{2.6a}$$

$$\partial_z \phi = (\partial_z f_m)\psi_m \tag{2.6b}$$

for $m = 1, 2 \ldots M$. Since our interest is in waves propagating in the coastal zone, where bed slopes are typically small, we restrict ourselves to mildly sloping beds. The bed slopes ∇h_0 and parameter derivatives $\nabla\kappa_m$ then are neglected when approximating the horizontal and vertical flow velocities, $\nabla\phi$ and $\partial_z\phi$, in the Hamiltonian density H. If the mild-slope assumption is not imposed, additional terms appear in the (still positive-definite) Hamiltonian density H and in the resulting flow equations. These

extra terms are of importance for wave reflections and in the case of rather steep slopes (Dingemans & Klopman 2009).

Using the mild slope approximation, (2.6) simplify to

$$\nabla\phi \approx \nabla\varphi + f_m\nabla\psi_m + (\partial_\zeta f_m)\psi_m\nabla\zeta, \tag{2.7a}$$

$$\partial_z\phi = (\partial_z f_m)\psi_m \tag{2.7b}$$

for $m = 1, 2 \ldots M$. When applied in (2.1b), a positive-definite Hamiltonian density $H(\zeta, \varphi, \psi_m; \boldsymbol{x}, t)$ will be the result. Furthermore, the cross-space z is integrated out, and the resulting system is only a function of the propagation space $\boldsymbol{x}$ and time t. Since, in our approximation, the highest spatial derivatives in the Hamiltonian density H are (quadratics of) first derivatives, the highest derivatives in the potential flow equations (2.5) will be second-order spatial derivatives. No mixed time–space derivatives appear. As we will see later, (2.5b) is, for given ζ and φ, a set of coupled linear second-order elliptic equations in the additional functions ψ_m, $m = 1, 2 \ldots M$.

While the above equations (2.5) are in terms of the surface potential φ, it is also possible to express them in terms of the surface-potential gradient $\boldsymbol{u} \equiv \nabla\varphi$. Note that $\boldsymbol{u}$ is not equal to the horizontal flow velocity $\nabla\phi$ at the free surface, i.e. $\boldsymbol{u} = [\nabla\phi]_{z=\zeta} + [\partial_z\phi]_{z=\zeta}\nabla\zeta$. After replacing $\nabla\varphi$ with $\boldsymbol{u} = (u_1, u_2)^T$ in the Hamiltonian $\mathscr{H}$, we get the following Hamiltonian system:

$$\partial_t\zeta = -\nabla\cdot\frac{\delta\mathscr{H}}{\delta\boldsymbol{u}} \qquad \text{and} \qquad \partial_t\boldsymbol{u} = -\nabla\frac{\delta\mathscr{H}}{\delta\zeta}, \tag{2.8}$$

under the additional requirement that each $\delta\mathscr{H}/\delta\psi_m = 0$ for all $m = 1, 2 \ldots M$. As for all Boussinesq models, the Laplace equation is no longer satisfied exactly in the fluid interior. So while the flow is still irrotational, the fluid is no longer exactly incompressible. However, as can be seen from the equation for $\partial_t\zeta$ in (2.8), we still have depth-integrated mass conservation (also in the velocity-potential formulation). Notice that an extension to flow with vorticity can easily be carried out using Shepherd (1990, equation (4.45)).

As a practical and simple application of the above approach, we will next consider the example of a single parabolic shape function ($M = 1$), which we will call hereafter the parabolic structure model. Next, we will continue with the more general case of several shape functions ($M > 1$). Finally, we discuss the case of a hyperbolic-cosine shape function (to be called the cosh or hyperbolic-cosine structure model in the remainder).

3. Parabolic structure model

Boussinesq (1872), for the case of a horizontal bottom, expressed the velocity potential ϕ as a series in the z direction around the bed level $z = -h_0$. Due to the impermeability of the bed, the vertical velocity $\partial_z\phi$ will be zero at the bed level $z = -h_0$. Then, to lowest order, the first deviation from a depth-uniform potential will be a parabolic contribution, in terms of the distance $z + h_0$ to the bed. Therefore, as a simple vertical structure model, we take $M = 1$ in (2.4a) and a parabolic shape function $f^{(p)}(z; \zeta, h_0)$:

$$f^{(p)}(z; \zeta, h_0) = \frac{1}{2}\,(z - \zeta\,)\,\frac{2h_0 + z + \zeta}{h_0 + \zeta}, \tag{3.1}$$

satisfying $\partial_z f^{(p)} = 0$ at the bed $z = -h_0$ and $f^{(p)} = 0$ at the free surface $z = \zeta$. Further $f^{(p)}$ has been scaled in such a way that the associated parameter $\psi^{(p)}(\boldsymbol{x}, t)$ equals the vertical velocity $\partial_z\phi$ at the free surface. It is assumed that the above parabolic

structure model is also a good approximation for the vertical flow structure in the case of mild bottom slopes.

For shortness of notation, we introduce the total water depth $h(\boldsymbol{x},t) \equiv h_0(\boldsymbol{x}) + \zeta(\boldsymbol{x},t)$. The Hamiltonian density $H^{(p)}(\zeta,\varphi,\psi^{(p)};\boldsymbol{x},t)$ becomes, for the parabolic shape function (3.1), after vertical integration using (2.7) and (2.1*b*):

$$H^{(p)} = \frac{1}{2}h\left(\nabla\varphi - \frac{2}{3}\psi^{(p)}\nabla\zeta - \frac{1}{3}h\nabla\psi^{(p)}\right)^2 + \frac{1}{90}h\left(\psi\,\nabla\zeta - h\,\nabla\psi^{(p)}\right)^2 + \frac{1}{6}h\left(\psi^{(p)}\right)^2 + \frac{1}{2}g\,\zeta^2, \quad (3.2)$$

which indeed is positive definite, since the water depth h is always positive. Note that the Hamiltonian density is fully nonlinear: no approximations have been made apart from the form and number of the shape functions, and the mild-slope approximation. The latter is only for convenience and is not essential to the method.

Taking the variations of the Hamiltonian $\mathscr{H} = \iint H\,\mathrm{d}\boldsymbol{x}$, the flow equations (2.5) become, after some rearrangements:

$$\partial_t\zeta + \nabla\cdot\left(h\boldsymbol{U}^{(p)}\right) = 0, \quad (3.3a)$$

$$\partial_t\varphi + \frac{1}{2}\left(\boldsymbol{U}^{(p)}\right)^2 - \frac{1}{45}\left(\psi^{(p)}\nabla\zeta + h\,\nabla\psi^{(p)}\right)^2 + \frac{1}{6}\left(1+\frac{1}{5}(\nabla\zeta)^2\right)\left(\psi^{(p)}\right)^2 + \nabla\cdot\left[h\left(\frac{2}{3}\nabla\varphi - \frac{7}{15}\psi^{(p)}\nabla\zeta - \frac{1}{5}h\,\nabla\psi^{(p)}\right)\psi^{(p)}\right] + g\zeta = 0, \quad (3.3b)$$

$$h\psi^{(p)}\left(\frac{1}{3}+\frac{7}{15}(\nabla\zeta)^2\right) - \left(\frac{2}{3}h\nabla\varphi - \frac{1}{5}h^2\nabla\psi^{(p)}\right)\cdot\nabla\zeta + \nabla\cdot\left(\frac{1}{3}h^2\nabla\varphi - \frac{1}{5}h^2\psi^{(p)}\nabla\zeta - \frac{2}{15}h^3\nabla\psi^{(p)}\right) = 0, \quad (3.3c)$$

where $\boldsymbol{U}^{(p)}(\boldsymbol{x},t)$ is the depth-averaged velocity:

$$\boldsymbol{U}^{(p)} = \nabla\varphi - \frac{2}{3}\psi^{(p)}\nabla\zeta - \frac{1}{3}h\nabla\psi^{(p)}. \quad (3.4)$$

For one spatial dimension, these equations are the same as those derived in Klopman, Dingemans & van Groesen (2005). So (3.3*a*, *b*) are the mass-conservation equation for the time evolution of ζ and a Bernouilli-like equation for the surface potential φ. Further, we have to solve a linear elliptic equation (3.3*c*) in terms of $\psi^{(p)}$, for given ζ and φ.

Later, in § 6, we will give the results of some numerical simulations using equations (3.3) in one spatial dimension. The linear characteristics of the parabolic structure model, i.e. linear dispersion and shoaling, will be derived in § 5.

4. General series model

Now we treat the general case of a vertical velocity-potential structure, as given in (2.4). By carefully choosing a small number M of shape functions $f_m(z;h_0,\zeta,\kappa_m)$, $m = 1\ldots M$, one aims at getting a good approximation to the exact vertical flow

structure. Using (2.7) in (2.5), we find for $H(\zeta, \varphi, \psi_m; \boldsymbol{x}, t)$:

$$\begin{aligned} H = & \frac{1}{2}\,(h_0+\zeta)\,(\nabla\varphi)^2 \\ & + \frac{1}{2}\,F_{mn}\,(\nabla\psi_m)\cdot(\nabla\psi_n) + \frac{1}{2}\,G_{mn}\psi_m\psi_n\,(\nabla\zeta)^2 + \frac{1}{2}\,K_{mn}\psi_m\psi_n \\ & + P_m\,(\nabla\psi_m)\cdot(\nabla\varphi) + Q_m\psi_m\,(\nabla\varphi)\cdot(\nabla\zeta) + R_{mn}\psi_n\,(\nabla\psi_m)\cdot(\nabla\zeta) \\ & + \frac{1}{2}g\zeta^2, \end{aligned} \tag{4.1}$$

where the integrals therein are defined by

$$F_{mn}(\zeta, h_0; \kappa_m, \kappa_n) = \int_{-h_0}^{\zeta} f_m f_n \,\mathrm{d}z = F_{nm}, \tag{4.2a}$$

$$G_{mn}(\zeta, h_0; \kappa_m, \kappa_n) = \int_{-h_0}^{\zeta} (\partial_\zeta f_m)(\partial_\zeta f_n)\,\mathrm{d}z = G_{nm}, \tag{4.2b}$$

$$K_{mn}(\zeta, h_0; \kappa_m, \kappa_n) = \int_{-h_0}^{\zeta} (\partial_z f_m)(\partial_z f_n)\,\mathrm{d}z = K_{nm}, \tag{4.2c}$$

$$P_m(\zeta, h_0; \kappa_m) = \int_{-h_0}^{\zeta} f_m \,\mathrm{d}z, \tag{4.2d}$$

$$Q_m(\zeta, h_0; \kappa_m) = \int_{-h_0}^{\zeta} (\partial_\zeta f_m)\,\mathrm{d}z, \tag{4.2e}$$

$$R_{mn}(\zeta, h_0; \kappa_m, \kappa_n) = \int_{-h_0}^{\zeta} f_m(\partial_\zeta f_n)\,\mathrm{d}z. \tag{4.2f}$$

Taking the variations of $\mathscr{H}$, as required by the Hamiltonian system (2.5), and keeping in mind that the coefficients as given in (4.2) also depend on $\zeta(\boldsymbol{x}, t)$, gives the following flow equations:

$$\partial_t\zeta + \nabla\cdot[(h_0+\zeta)\,\nabla\varphi + P_m\,\nabla\psi_m + Q_m\,\psi_m\nabla\zeta] = 0, \tag{4.3a}$$

$$\partial_t\varphi + \frac{1}{2}\,(\nabla\varphi)^2 + g\,\zeta + \mathscr{R} = 0 \tag{4.3b}$$

and

$$\begin{aligned} & [G_{lm}\,(\nabla\zeta)^2 + K_{lm}]\,\psi_m + Q_l\,(\nabla\varphi)\cdot(\nabla\zeta) + R_{ml}\,(\nabla\psi_m)\cdot(\nabla\zeta) \\ & \qquad - \nabla\cdot(F_{lm}\,\nabla\psi_m + P_l\,\nabla\varphi + R_{lm}\,\psi_m\,\nabla\zeta) = 0 \quad \text{for } l = 1\ldots M, \end{aligned} \tag{4.3c}$$

where the non-hydrostatic term $\mathscr{R}(\boldsymbol{x}, t)$ is given by

$$\begin{aligned} \mathscr{R} = & \frac{1}{2}\,F'_{mn}\,(\nabla\psi_m)\cdot(\nabla\psi_n) + \frac{1}{2}\,[G'_{mn}\,(\nabla\zeta)^2 + K'_{mn}]\,\psi_m\,\psi_n + [P'_m\,\nabla\psi_m + Q'_m\,\psi_m\,\nabla\zeta]\cdot\nabla\varphi \\ & + R'_{mn}\,(\nabla\zeta)\cdot(\nabla\psi_m)\,\psi_n - \nabla\cdot[G_{mn}\,\psi_m\,\psi_n\,\nabla\zeta + Q_m\,\psi_m\,\nabla\varphi + R_{mn}\,(\nabla\psi_m)\,\psi_n]. \end{aligned} \tag{4.4}$$

Here a prime denotes variation with respect to $\zeta(x, t)$, e.g. $K'_{mn} \equiv \delta K_{mn}/\delta\zeta$. Observe that, as a result of $f_m = 0$ at $z = \zeta(x, t)$, we have

$$F'_{mn} = R_{mn} + R_{nm} \qquad \text{and} \qquad P'_m = Q_m. \tag{4.5}$$

As before, for the parabolic structure model, we have a mass conservation equation (4.3*a*), a Bernoulli equation (4.3*b*) and a series of second-order elliptic equations (4.3*c*), linear in ψ_m. The highest derivatives are second-order spatial derivatives. For numerical applications, the solution of the elliptic equations requires that they are well conditioned, i.e. that the lth elliptic equation is independent of the nth equation, for $l \neq n$. Therefore these shape functions f_m have to be sufficiently independent of each other. This may pose restrictions on the choice of the shape functions f_m, as well as the maximum number of shape functions M. See, for example, Dommermuth & Yue (1987), where the computations only converged for a small number of shape functions.

Fortunately, in general, only a small number of well-chosen shape functions is sufficient to get good approximate models. Often, using only one shape function, i.e. $M = 1$, may already give good results. In the remainder, we will treat a few examples. Besides the parabolic structure model, with shape function $f^{(p)}(z;\zeta, h_0)$ and presented in § 3, we will discuss two other examples: a cosh (hyperbolic-cosine) structure model and a power-series structure model.

4.1. *Hyperbolic-cosine structure model*

First, one possibility is to exploit the well-known hyperbolic-cosine vertical structure as found in the full linear wave theory:

$$f^{(c)}(z;\zeta, h_0, \kappa) = \cosh \kappa\ (h_0 + z) - \cosh \kappa\ (h_0 + \zeta), \tag{4.6}$$

where $\kappa(\boldsymbol{x})$ is an additional parameter, which can be chosen for instance on the basis of the carrier-wave angular frequency ω_0 of incoming waves and the local water depth $h_0(\boldsymbol{x})$, using the linear dispersion relationship.

The vertical integrals (4.2), as well as their ζ-derivatives, valid for the cosh and power-series structure models are given in the Appendix. Then the associated Hamiltonian density $H^{(c)}(\zeta, \varphi, \psi^{(c)}; \boldsymbol{x}, t)$, using (4.1), becomes after some manipulations:

$$H^{(c)} = \frac{1}{2} h \left(\nabla\varphi - \mathscr{D}\nabla\psi^{(c)} - \kappa\, \mathscr{S}\psi^{(c)}\nabla\zeta\right)^2 + \frac{1}{4}\frac{1}{\kappa}\left(\kappa h + \mathscr{S}\mathscr{C} - 2\frac{\mathscr{S}^2}{\kappa h}\right)\left(\nabla\psi^{(c)}\right)^2 + \frac{1}{4}\kappa\left(\mathscr{S}\mathscr{C} - \kappa h\right)\left(\psi^{(c)}\right)^2 + \frac{1}{2} g\, \zeta^2 \tag{4.7}$$

with

$$\mathscr{D} \equiv \cosh(\kappa h) - \frac{\sinh(\kappa h)}{\kappa h}, \quad \mathscr{S} \equiv \sinh(\kappa h) \quad \text{and} \quad \mathscr{C} \equiv \cosh(\kappa h). \tag{4.8}$$

The Hamiltonian density $H^{(c)}$ is indeed positive definite, since the coefficients in front of $(\nabla\psi)^2$ and $(\psi^{(c)})^2$, in the second and third term on the right-hand side, are always positive for $\kappa > 0$ and $h > 0$. When the integrals from (A 2) are applied to (4.3), we

get after some algebraic manipulations:

$$\partial_t \zeta + \nabla \cdot \left(h \boldsymbol{U}^{(c)}\right) = 0, \tag{4.9a}$$

$$\partial_t \varphi + \frac{1}{2}\left(\boldsymbol{U}^{(c)}\right)^2 + \frac{1}{2}\kappa^2 \mathscr{S}^2 \left(\psi^{(c)}\right)^2 + \frac{1}{2}\mathscr{D}^2 \left(\nabla \psi^{(c)}\right)^2 - \kappa h \boldsymbol{U}^{(c)} \cdot \left[\left(\mathscr{S} - \frac{\mathscr{D}}{\kappa h}\right)\nabla \psi^{(c)} + \kappa\, \mathscr{C} \psi^{(c)} \nabla \zeta\right] + \nabla \cdot \left(\kappa\, h \mathscr{S} \boldsymbol{U}^{(c)} \psi^{(c)}\right) + g\zeta = 0, \tag{4.9b}$$

$$-\kappa\, h \mathscr{S}\left(\nabla \varphi - \mathscr{D} \nabla \psi^{(c)} - \kappa\, \mathscr{S} \psi^{(c)} \nabla \zeta\right) \cdot \nabla \zeta + \frac{1}{2}\kappa\left(\mathscr{S}\mathscr{C} - \kappa\, h\right) \psi^{(c)} + \nabla \cdot \left[h \mathscr{D}\left(\nabla \varphi - \kappa\, \mathscr{S} \psi^{(c)} \nabla \zeta\right) + \frac{1}{\kappa}\left(\frac{\mathscr{S}^2}{\kappa h} - \mathscr{D}^2 \kappa\, h - \frac{1}{2}\kappa\, h - \frac{1}{2}\mathscr{S}\mathscr{C}\right)\nabla \psi^{(c)}\right] = 0, \tag{4.9c}$$

where $\boldsymbol{U}^{(c)}(\boldsymbol{x}, t)$ is the depth-averaged velocity:

$$\boldsymbol{U}^{(c)} \equiv \nabla \varphi - \mathscr{D} \nabla \psi^{(c)} - \kappa \mathscr{S} \psi^{(c)} \nabla \zeta. \tag{4.10}$$

We did not use $\boldsymbol{U}^{(c)}$ in (4.9*c*), since this is basically an elliptic equation in terms of $\psi^{(c)}$ and $\boldsymbol{U}^{(c)}$ depends on $\psi^{(c)}$.

4.2. *Power-series structure model*

Second, in the power-series structure model, we use for the vertical shape functions a power-series expansion around the free surface $z = \zeta(x, t)$. So,

$$f_m^{(s)} = (z - \zeta(\boldsymbol{x}, t))^m, \qquad \text{with } m = 1 \ldots M. \tag{4.11}$$

This can be seen as a generalization of the parabolic structure model. Through the choice of the expansion around the free surface, the still water depth h_0 is not present in the shape functions. For this particular choice, the last two terms of (2.6*a*) disappear. So, (2.7*a*) is exact. The bottom-slope terms in the flow equations now appear through the variations of the Hamiltonian. Because no explicit approximation in the bottom-slope terms has been made, we have not made a mild-slope assumption in this case. The integrals, required in the Hamiltonian density (2.1*b*) and in the flow equations (4.3), are given by (A 4).

We do not yet know the maximum value of M for which the shape functions $f_m^{(s)}$ are sufficiently independent of each other, in order that the numerical approximation to the flow equations will result in a well-conditioned set of equations. Convergence may be improved by using orthogonal Chebychev polynomials instead of the simple power series resulting from (4.11).

Some linear characteristics of the variational Boussinesq model, i.e. the linear dispersion characteristics and the linear shoaling behaviour, will be derived in the next section. They will be applied to the three given examples with parabolic, cosh and power-series shape functions.

5. Linear wave characteristics from the average Lagrangian

5.1. *Average Lagrangian for linear waves*

The linear frequency dispersion and shoaling of the variational Boussinesq model is studied. Since we have a variational model, we apply the average Lagrangian technique (see e.g. Whitham 1974, § 11.7 and chapter 14) to the one-dimensional linearized wave equations. This leads, due to the invariance with respect to wave phase, to a wave

action equation (Hayes 1970*a*,*b*, 1973; Whitham 1974). For time-periodic waves, the invariance of the wave action flux provides the shoaling characteristics. The present analysis method is easier to apply than the direct manipulations of Boussinesq equations by a method due to Wentzel, Kramers, Brilliouin and Jeffreys (known as the WKBJ method) (Madsen & Sørensen 1992; Dingemans 1997, §§ 5.5.8 and 5.5.9; Ludwig 1970). Furthermore, the variational approach gives a direct representation of the 'global' (integral) effects of shoaling from one location to another, using the invariance of the action flux. Previous WKBJ approaches give 'local' changes, associated, in our case, with the spatial derivative of the wave action flux. Chen & Liu (1995) integrate the local shoaling characteristics to obtain the global shoaling behaviour. It is not clear *a priori* that the integration of the local shoaling behaviour gives a conservation law for the energy flux in many Boussinesq models. In our case the conservation of wave action is guaranteed, because we start with a variational model.

For a linear problem with one spatial dimension x, the Lagrangian will be a second-degree polynomial in terms of ζ, φ, ψ and their derivatives. So, for the linear wave problem the Lagrangian and Hamiltonian densities, L_0 and H_0 respectively, become by use and reduction of (2.1) and (4.1):

$$L_0 = \varphi \partial_t \zeta - H_0, \tag{5.1a}$$

$$H_0 = \frac{1}{2} h_0 (\partial_x \varphi)^2 + \frac{1}{2} \overline{F}_{mn} (\partial_x \psi_m)(\partial_x \psi_n) + \frac{1}{2} \overline{K}_{mn} \psi_m \psi_n + \overline{P}_m (\partial_x \psi_m)(\partial_x \varphi) + \frac{1}{2} g \zeta^2 \tag{5.1b}$$

with the overbar denoting evaluation of the quantity at $\zeta = 0$. By taking variations of

$$\mathscr{L}_0(\zeta, \varphi, \psi_m) \equiv \iint L_0(\zeta, \varphi, \psi_m; x, t)\, \mathrm{d}x\, \mathrm{d}t \tag{5.2}$$

with respect to $\varphi(x,t)$, $\zeta(x,t)$ and $\psi_l(x,t)$, we get from $\delta \mathscr{L}_0 = 0$:

$$\partial_t \zeta + \partial_x (h_0 \partial_x \varphi + \overline{P}_m \partial_x \psi_m) = 0, \tag{5.3a}$$

$$\partial_t \varphi + g \zeta = 0, \tag{5.3b}$$

$$\overline{K}_{lm} \psi_m - \partial_x (\overline{F}_{lm} \partial_x \psi_m + \overline{P}_l \partial_x \varphi) = 0, \qquad \text{for } l = 1, 2 \ldots M. \tag{5.3c}$$

We use the average Lagrangian technique of Whitham (1974) to study the linear dispersion and shoaling characteristics of the equations.

Assuming slowly modulated waves, we use the following approximation for $\zeta(x,t)$, $\varphi(x,t)$ and $\psi_m(x,t)$:

$$\zeta(x,t) = a(\mu x, \mu t) \cos \theta(x,t), \qquad \varphi(x,t) = b(\mu x, \mu t) \sin \theta(x,t), \tag{5.4a}$$

$$\psi_m(x,t) = c_m(\mu x, \mu t) \sin \theta(x,t), \qquad \text{for } m = 1, 2 \ldots M, \tag{5.4b}$$

in agreement with the solution of (5.3) for progressive harmonic waves over a horizontal bed. Here, $\mu \ll 1$ is a small modulation parameter and $\theta(x,t)$ is the wave phase. Neglecting derivatives of the amplitudes $a(\mu x, \mu t)$, $b(\mu x, \mu t)$ and $c(\mu x, \mu t)$, since they are $O(\mu)$ compared to the leading-order terms, we have

$$\partial_t \zeta \approx \omega a \sin \theta, \quad \partial_x \varphi \approx k b \cos \theta \quad \text{and} \quad \partial_x \psi_m \approx k c_m \cos \theta, \tag{5.5}$$

with the angular wave frequency $\omega(x,t)$ and wavenumber $k(x,t)$ defined as

$$\omega \equiv -\partial_t \theta \qquad \text{and} \qquad k \equiv +\partial_x \theta. \tag{5.6}$$

The linear approximations (5.4) and (5.5) are used in (5.1) to compute the Lagrangian density $L_0(a, b, c_m, \theta; x, t)$. Next, Whitham (1974) introduces the average Lagrangian density $\langle L_0 \rangle (a, b, c_m, \theta; x, t)$ as

$$\langle L_0 \rangle = \frac{1}{2\pi} \int_0^{2\pi} L_0 \, \mathrm{d}\theta. \tag{5.7}$$

For slowly varying wave fields with negligible reflection, this can be assumed to give a good description. In our case, we get for the average Lagrangian density $\langle L_0 \rangle$ and (positive definite) average Hamiltonian density $\langle H_0 \rangle$:

$$\langle L_0 \rangle = \frac{1}{2} \omega \, a \, b - \langle H_0 \rangle \tag{5.8a}$$

with

$$\langle H_0 \rangle = \frac{1}{4} k^2 h_0 \, b^2 + \frac{1}{4} (\overline{F}_{mn} \, k^2 + \overline{K}_{mn}) \, c_m \, c_n + \frac{1}{2} \overline{P}_m \, k^2 \, b \, c_m + \frac{1}{4} g \, a^2. \tag{5.8b}$$

Using the variations of $\langle \mathscr{L}_0 \rangle (a, b, c_m) = \iint \langle L_0 \rangle \, \mathrm{d}x \, \mathrm{d}t$ with respect to $a(\mu x, \mu t)$ and $c_l(\mu x, \mu t)$, we get

$$b = \frac{g}{\omega} a \quad \text{and} \quad (\overline{K}_{lm} + k^2 \overline{F}_{lm}) c_m = - \frac{g}{\omega} k^2 \overline{P}_l a \tag{5.9}$$

for $l = 1, 2 \ldots M$. The last equation can be written in matrix form as

$$(\overline{\boldsymbol{K}} + k^2 \overline{\boldsymbol{F}}) \boldsymbol{c} = - \frac{g}{\omega} k^2 \overline{\boldsymbol{p}} a. \tag{5.10}$$

Because of the positive-definite Hamiltonian $\langle \mathscr{H}_0 \rangle (a, b) = \int \langle H_0 \rangle \, \mathrm{d}x$, this matrix equation is invertible. With $\overline{\boldsymbol{W}}$ denoting the inverse of the matrix in front of $\boldsymbol{c}$, we can write

$$\boldsymbol{c} = - \frac{g}{\omega} k^2 \overline{\boldsymbol{W}} \, \overline{\boldsymbol{p}} a, \quad \text{where} \quad \overline{\boldsymbol{W}} \equiv (\overline{\boldsymbol{K}} + k^2 \overline{\boldsymbol{F}})^{-1} \tag{5.11a}$$

or, in component form,

$$c_m = - \frac{g}{\omega} k^2 \overline{W}_{mn} \, \overline{P}_n a \quad \text{for} \quad m = 1, 2 \ldots M. \tag{5.11b}$$

Note from (5.10) that $\overline{W}_{mn}$ will be a rational function in terms of k^2. Applying these to the average Lagrangian density $\langle L_0 \rangle$, (b) and c_m can be eliminated from $\langle L_0 \rangle$, and we get after some algebraic manipulations:

$$\langle L_0 \rangle = \frac{1}{4} \left\{ 1 - (k \, h_0)^2 \left[1 - (k \, h_0)^2 \, \frac{\overline{W}_{mn} \, \overline{P}_m \, \overline{P}_n}{h_0^3} \right] \frac{g}{\omega^2 \, h_0} \right\} g a^2. \tag{5.12}$$

This will be used consecutively to find the linear dispersion and shoaling characteristics.

5.2. *Linear dispersion*

As is well known (Hayes 1970*a*,*b*, 1973; Whitham 1974, § 11.7), for linear waves the average Lagrangian density $\langle L_0 \rangle$ has the form

$$\langle L_0 \rangle = D(\omega, k) a^2 \tag{5.13}$$

with $D(\omega, k)$ the dispersion relationship. So variation with respect to $a(\mu x, \mu t)$ directly gives the linear dispersion relation $D(\omega, k) = 0$. In our case, we have from the terms

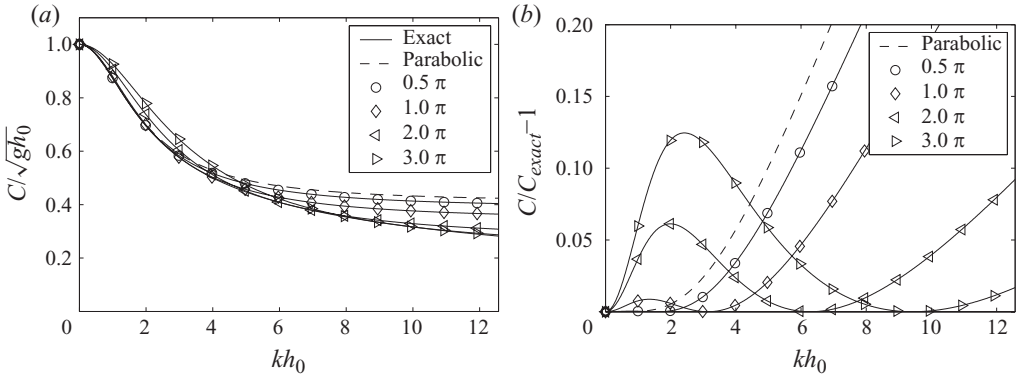

FIGURE 1. Linear dispersion characteristics of the parabolic and cosh structure model as a function of kh_0. (*a*) Phase speed $C/\sqrt{g\,h_0}$ (with $C \equiv \Omega/k$) in the cosh structure model (solid lines with markers) versus the exact linear phase speed (solid line, lowest curve) and the parabolic structure model (dashed line). (*b*) Relative error $C/C_{exact} - 1$ (on a linear scale) in the phase speed of the cosh structure model (solid lines) and the parabolic structure model (black dashed line). The markers are for different values of κh_0: $\pi/2$ (–○–), π (–◇–), 2π (–◁–) and 3π (–▷–).

between curly brackets in (5.12) being equal to zero:

$$\omega = \Omega(k, h_0) \quad \text{with} \quad \frac{\Omega^2 h_0}{g} \equiv (k h_0)^2 \left[1 - (k h_0)^2 \frac{\overline{W}_{mn}\, \overline{P}_m\, \overline{P}_n}{h_0^3} \right]. \tag{5.14}$$

Further, we introduce the phase speed $C \equiv \Omega(k)/k$, for which we find

$$\frac{C^2}{g h_0} = \left[1 - (k h_0)^2 \frac{\overline{W}_{mn}\, \overline{P}_m\, \overline{P}_n}{h_0^3} \right]. \tag{5.15}$$

For example, consider the parabolic structure model, which has $M = 1$, so, using the integrals in the Appendix evaluated at $\zeta = 0$:

$$\overline{F}^{(p)} = \frac{2}{15} h_0^3, \quad \overline{K}^{(p)} = \frac{1}{3} h_0 \quad \text{and} \quad \overline{P}^{(p)} = -\frac{1}{3} h_0^2. \tag{5.16}$$

From (5.10), (5.11) and (5.14) we find for the linear dispersion relationship:

$$\frac{\left(C^{(p)}\right)^2}{g h_0} = \frac{1 + \dfrac{1}{15} k^2 h_0^2}{1 + \dfrac{2}{5} k^2 h_0^2}. \tag{5.17}$$

This is the same dispersion relation as for the Boussinesq equations with improved linear dispersion of Madsen *et al.* (1991, equation (15) for the case $B = 1/15$). The linear dispersion characteristics, as compared with the exact result for the full linear theory,

$$\frac{C_{exact}^2}{g h_0} = \frac{\tanh k h_0}{k h_0}, \tag{5.18}$$

are shown in figure 1, up to $kh_0 = 4\pi$ (which corresponds to a water depth of twice the wavelength, i.e. deep water). Up to $kh_0 = \pi$ the relative error in the phase speed is less than 3 %.

In our second example, the cosh structure model, we have from (4.6) and (A 2) for the required integrals:

$$\overline{F}^{(c)} = -\frac{3}{2}\frac{1}{\kappa}\overline{\mathscr{S}}\,\overline{\mathscr{C}} + \frac{1}{2}h_0 + h_0\overline{\mathscr{C}}^2, \qquad \overline{K}^{(c)} = \frac{1}{2}\kappa\overline{\mathscr{S}}\,\overline{\mathscr{C}} - \frac{1}{2}\kappa^2 h_0, \qquad \overline{P}^{(c)} = -h_0\overline{\mathscr{D}} \tag{5.19}$$

with $\overline{\mathscr{D}} \equiv \cosh(\kappa h_0) - (\sinh(\kappa h_0)/\kappa h_0)$, $\overline{\mathscr{S}} \equiv \sinh(\kappa h_0)$ and $\overline{\mathscr{C}} \equiv \cosh(\kappa h_0)$. Using these in (5.10), (5.11) and (5.14), we find

$$\frac{\left(C^{(c)}\right)^2}{g h_0} = \frac{\left(\dfrac{\overline{\mathscr{S}}\,\overline{\mathscr{C}}}{\kappa h_0} - 1\right)\left(1 - \dfrac{k^2}{\kappa^2}\right) + 2\dfrac{k^2}{\kappa^2}\dfrac{\overline{\mathscr{S}}}{\kappa h_0}\overline{\mathscr{D}}}{\left(\dfrac{\overline{\mathscr{S}}\,\overline{\mathscr{C}}}{\kappa h_0} - 1\right)\left(1 - \dfrac{k^2}{\kappa^2}\right) + 2\dfrac{k^2}{\kappa^2}\overline{\mathscr{C}}\,\overline{\mathscr{D}}}. \tag{5.20}$$

As can be seen from this approximate dispersion relation, we regain the exact value of the linear dispersion relation at $k = \kappa$. Also the group velocity $V = \partial_k \Omega$ is exact at $k = \kappa$, i.e. $\partial_k \Omega^{(c)}(\kappa) = \partial_k \Omega_{exact}(\kappa)$. The linear dispersion characteristics and associated errors (as compared to the full linear theory) for the cosh structure model are shown in figure 1. The fact that the dispersion errors are small both near $kh_0 = \kappa h_0$ and near $kh_0 = 0$ is advantageous for the study of narrow-banded nonlinear wave groups, where besides the carrier waves with wavenumbers approximately equal to k_0, there are also subharmonics present with wavenumbers near zero. This is also a desirable feature when studying the interaction between (very) long waves and shorter waves. Further note that $\kappa(x)$ can be a spatially varying parameter, and may be chosen differently at different locations to best facilitate the local conditions, i.e. local still water-depth h_0 and carrier wavenumber k_0.

Next, we consider the power-series structure model (4.11). Here, for $M > 1$, we have to solve (5.10) using the integrals as given in (A 4). For some small values of M we have done this (using the MAPLE symbolic algebraic manipulator), and as a result we obtained the following dispersion characteristics, with $q \equiv kh_0$:

$$\frac{\left(C_1^{(s)}\right)^2}{g h_0} = \frac{1 + \dfrac{1}{12}q^2}{1 + \dfrac{1}{3}q^2}, \tag{5.21a}$$

$$\frac{\left(C_2^{(s)}\right)^2}{g h_0} = \frac{1 + \dfrac{1}{10}q^2 + \dfrac{1}{720}q^4}{1 + \dfrac{13}{30}q^2 + \dfrac{1}{80}q^4}, \tag{5.21b}$$

$$\frac{\left(C_3^{(s)}\right)^2}{g h_0} = \frac{1 + \dfrac{13}{105}q^2 + \dfrac{1}{420}q^4 + \dfrac{1}{100800}q^6}{1 + \dfrac{16}{35}q^2 + \dfrac{3}{140}q^4 + \dfrac{1}{6300}q^6}, \tag{5.21c}$$

$$\frac{\left(C_4^{(s)}\right)^2}{g h_0} = \frac{1 + \dfrac{17}{126}q^2 + \dfrac{11}{3024}q^4 + \dfrac{1}{42336}q^6 + \dfrac{1}{25401600}q^8}{1 + \dfrac{59}{126}q^2 + \dfrac{19}{720}q^4 + \dfrac{5}{14112}q^6 + \dfrac{1}{1016064}q^8}, \tag{5.21d}$$

$$\frac{\left(C_5^{(s)}\right)^2}{g h_0} = \frac{1 + \dfrac{14}{99}q^2 + \dfrac{373}{83160}q^4 + \dfrac{1}{22680}q^6 + \dfrac{1}{7983360}q^8 + \dfrac{1}{10059033600}q^{10}}{1 + \dfrac{47}{99}q^2 + \dfrac{163}{5544}q^4 + \dfrac{16}{31185}q^6 + \dfrac{67}{23950080}q^8 + \dfrac{1}{279417600}q^{10}}. \tag{5.21e}$$

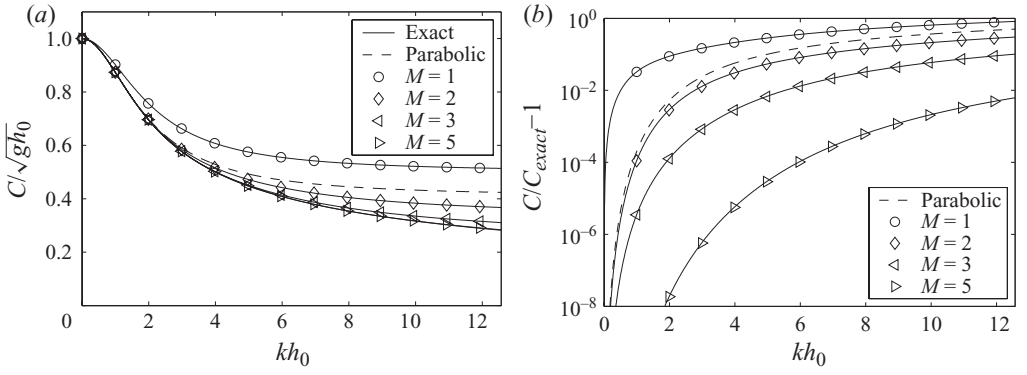

FIGURE 2. Linear dispersion characteristics of the power-series structure model as a function of kh_0. (*a*) Phase speed $C_M^{(s)}/\sqrt{g\,h_0}$ (with $C_M^{(s)} \equiv \Omega_M^{(s)}/k$) in the power-series structure model (solid lines with markers) versus the exact linear phase speed (solid line, lowest curve) and the parabolic structure model (dashed line). (*b*) Relative error $C_M^{(s)}/C_{exact} - 1$ (on a linear scale) in the phase speed of the cosh structure model (solid lines with markers) and the parabolic structure model (dashed line). The markers for different values of M are $M = 1$ (–○–), $M = 2$ (–◇–), $M = 3$ (–◁–) and $M = 5$ (–▷–).

Here $C_M^{(s)}(k, h_0)$ is the phase speed for the case with M terms in the power-series expansion. A comparison for the phase speed and the relative error therein is made in figure 2, as a function of the relative depth kh_0. As can be seen, for $M = 2$ the relative error $\varepsilon \equiv C_M^{(s)}/C_{exact} - 1$ is less than 0.01 for $kh_0 < 2.77$, i.e. for almost the whole range of shallow to deep-water waves (considering $kh_0 > \pi$ as deep water). For $M = 3$ and $M = 5$ the range where $\varepsilon < 0.01$ has extended to $kh_0 < 5.53$ and $kh_0 < 14.07$, respectively.

Concerning the accuracy of these phase velocities, we notice that these approximations are not the same as the Padé approximations to the exact linear phase velocity squared C_{exact}^2 (see (5.18)). For $M = 3$ the result is about the same as for the [4, 4] Padé approximation in terms of q, whereas it is not as accurate as the [6, 6] Padé (which has the same powers of q in the numerator and denominator). For $M = 4$ the accuracy is in between those of the [4, 4] and [6, 6] Padé approximations.

5.3. *Linear shoaling*

The linear shoaling characteristics are studied using the wave action equation, resulting from the variation of the average Lagrangian $\langle \mathscr{L}_0 \rangle \equiv \iint \langle L_0 \rangle \,\mathrm{d}x\,\mathrm{d}t$ with respect to the wave phase $\theta(x, t)$. Using (5.14), we can write the average Lagrangian density $\langle L_0 \rangle$, equation (5.12), as

$$\langle L_0 \rangle = \left(1 - \frac{\Omega^2(k, h_0)}{\omega^2}\right) \frac{1}{2} g a^2. \tag{5.22}$$

Note that through the phase averaging, the phase $\theta(x, t)$ itself no longer appears in the average Lagrangian density $\langle L_0 \rangle (a, k, \omega; x, t)$, equation (5.12), but only its derivatives $\omega \equiv -\partial_t \theta$ and $k \equiv +\partial_x \theta$. Consequently, the result is a conservation equation (Hayes 1970*a*,*b*, 1973; Whitham 1974):

$$\partial_t \mathscr{A} + \partial_x \mathscr{B} = 0 \tag{5.23}$$

with, using (5.22),

$$\mathscr{A} \equiv + \frac{\partial \langle L_0 \rangle}{\partial \omega} = \frac{\frac{1}{2} g a^2}{\omega} \qquad \text{and} \qquad \mathscr{B} \equiv - \frac{\partial \langle L_0 \rangle}{\partial k} = V \frac{\frac{1}{2} g a^2}{\omega}. \tag{5.24}$$

Here $\mathscr{A}(x,t)$ is the wave action, $\mathscr{B}(x,t)$ is the wave action flux. Further, $V(x,t) \equiv \partial\mathscr{B}/\partial\mathscr{A} = \mathscr{B}/\mathscr{A} = \partial_k \Omega$ is the group velocity (Hayes 1973), which depends on the dispersion characteristics of the specific variational Boussinesq model under consideration.

Now, when studying the linear shoaling behaviour for the variational Boussinesq model, we consider time-harmonic waves, i.e. the wave amplitude $a(x,t)$ is constant in time and the angular frequency ω is a constant. Hence $\partial_t \mathscr{A} = 0$, and (5.23) becomes

$$\partial_x (V \mathscr{A}) = 0. \tag{5.25}$$

As a result, we have that

$$\sqrt{V} a = \text{constant}, \tag{5.26}$$

when going from one depth $h_0(x)$ to another. So, when the wave has an amplitude $a_1 \equiv a(x_1)$ at location x_1, the wave amplitude at x_2 will be $a_2 = \sqrt{V_1/V_2} a_1$, with V_1 and V_2 the group velocity at x_1 and x_2, respectively.

As an example, we consider the parabolic structure model, with linear frequency dispersion given by (5.17). Consequently, the group velocity $V^{(p)} \equiv \partial_k \Omega^{(p)}$ for this model is

$$V^{(p)} = \frac{\Omega}{k} \left[1 - \frac{\frac{1}{3} k^2 h_0^2}{\left(1 + \frac{1}{15} k^2 h_0^2\right)\left(1 + \frac{2}{5} k^2 h_0^2\right)} \right]. \tag{5.27}$$

Note that in the shallow-water limit $kh_0 \to 0$ we have $V^{(p)} \to \sqrt{g h_0}$. And for the deep-water case $kh_0 \to \infty$ we have that $V^{(p)} \to \sqrt{g h_0/6}$.

This can be compared with the full linear theory, where we have for the group velocity V_{exact} (see e.g. Dingemans 1997, equation (2.29)):

$$V_{exact} = \frac{1}{2} \frac{\Omega_{exact}}{k} \left(1 + k h_0 \frac{1 - \tanh^2 k h_0}{\tanh k h_0} \right), \tag{5.28}$$

which has the shallow-water limit $V_{exact} / \sqrt{g h_0} \to 1$ for $kh_0 \to 0$ and the deep-water limit $V_{\text{exact}} / \sqrt{g/k} \to \frac{1}{2}$ for $kh_0 \to \infty$ (and keeping k fixed).

Considering again the parabolic structure model, the integral shoaling behaviour according to (5.26), and associated errors as compared with full linear theory, are depicted in figure 3. As can be seen, the agreement between the approximate model and the full linear theory result is quite good. For instance, for periodic waves propagating from a location with $kh_0 = \pi$ to a very shallow location ($kh_0 \to 0$), the relative error in the wave amplitude (a) at the shallow-water location is less than 10 %. And when starting at $kh_0 = \pi/2$, the shallow-water wave amplitude is less than 1 % in error with the full linear theory result.

A different approach to the study of linear wave shoaling, without demanding energy or action conservation, has been used by e.g. Madsen & Sørensen (1992) (and Dingemans 1997, § 5.5). They use a WKBJ method directly on the wave evolution equations themselves, ending up with a description of the 'local' shoaling behaviour, i.e. how $a'(x)/a(x)$ depends on $h_0'(x)/h_0(x)$, with $(\cdot)'$ denoting x-derivatives. Our

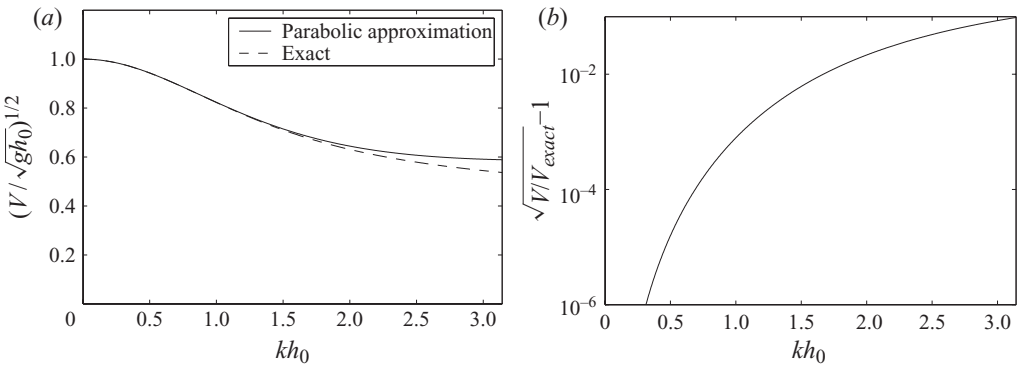

FIGURE 3. Linear shoaling behaviour of the parabolic structure model as a function of kh_0. (*a*) Square root of the relative group velocity $(V/\sqrt{gh_0})^{1/2}$, for the parabolic structure model (solid line) and according to the exact linear shoaling factor $(V_{exact}/\sqrt{gh_0})^{1/2}$ (dashed line). (*b*) Relative error $\sqrt{V/V_{exact}}-1$ on a semilogarithmic scale.

result is the same as for the Madsen & Sørensen (1992) model (see Dingemans 1997, equation (5.190)). This result has also been obtained by a local analysis using the method of Ludwig (1970) (see also Dingemans 1997, p. 569), on the flow equations (5.3) themselves. This is not surprising, since Bretherton (1968) has shown the correspondence between the conservation of wave action and the WKBJ approach for linear systems arising from a variational principle.

With regard to the cosh structure model, we can remark that since the group velocity is exact for $k = \kappa$, we can have exact linear shoaling for monochromatic waves with frequency ω_0, provided κ is chosen according to the local depth and the linear dispersion relation $\omega_0^2 = g\kappa \tanh \kappa h_0$. For the power-series structure model, the shoaling coefficient behaves in a similar fashion as for the parabolic structure model: the relative error in $\sqrt{V}$ is larger than the error in the phase speed C, but of the same order (typically two to five times as large). The analytical expressions for the group speed become quite lengthy for the cosh structure model and for the power-series structure model with $M \geqslant 3$, and will not be presented here.

6. Numerical simulations for the parabolic structure model

6.1. *Numerical method*

The parabolic structure model (3.3) in one spatial-dimension is used to study the applicability and nonlinear behaviour of the variational Boussinesq model numerically. Instead of the surface potential $\varphi(x,t)$, we work with its gradient $u(x,t) \equiv \partial_x \varphi$. So, the equations to be solved are, taking the x-derivative of (3.3*b*),

$$\partial_t \zeta + \partial_x \left(hU^{(p)}\right) = 0, \tag{6.1a}$$

$$\partial_t u + \partial_x \left\{ \frac{1}{2}\left(U^{(p)}\right)^2 + g\zeta - \frac{1}{45}\left(\psi^{(p)}\partial_x\zeta + h\,\partial_x\psi^{(p)}\right)^2 + \frac{1}{6}\left(1+\frac{1}{5}(\partial_x\zeta)^2\right)\left(\psi^{(p)}\right)^2 + \partial_x\left[h\left(\frac{2}{3}u - \frac{7}{15}\psi^{(p)}\partial_x\zeta - \frac{1}{5}h\,\partial_x\psi^{(p)}\right)\psi^{(p)}\right]\right\} = 0, \tag{6.1b}$$

$$h\psi^{(p)}\left(\frac{1}{3}+\frac{7}{15}(\partial_x\zeta)^2\right) - \left(\frac{2}{3}hu - \frac{1}{5}h^2\partial_x\psi^{(p)}\right)\partial_x\zeta + \partial_x\left(\frac{1}{3}h^2u - \frac{1}{5}h^2\psi^{(p)}\partial_x\zeta - \frac{2}{15}h^3\partial_x\psi^{(p)}\right) = 0 \tag{6.1c}$$

with the depth-averaged velocity

$$U^{(p)} = u - \frac{2}{3}\psi^{(p)}\partial_x\zeta - \frac{1}{3}h\partial_x\psi^{(p)}. \tag{6.2}$$

Note that the equations solved in the numerical model are dimensional.

We use the method of lines for the numerical solution of this set of partial differential equations: first the equations are discretized in space, and then the resulting sets of ordinary differential equations for the temporal evolution are marched in time. For the spatial discretization, a pseudo-spectral method is used on a periodic spatial domain. The flow quantities ζ, u and $\psi^{(p)}$, as well as the still water depth h_0, are discretized on a uniform grid of N intervals and step size Δx: $\zeta_{,j}$, $u_{,j}$, $\psi^{(p)}_{,j}$ and $h_{0,j}$ denote the respective quantities at location $x = j\,\Delta x$. Spatial derivatives of a quantity are computed in the Fourier wavenumber domain, using the fast Fourier transform (FFT) to switch back and forth between the spatial and the wavenumber domain.

As a result, (6.1*a*, *b*) become a set of N first-order ordinary differential equations for the time evolution of $\zeta_{,j}$ and $\varphi_{,j}$, $j = 1\ldots N$. These are marched in time using a variable step-size Runge–Kutta time integrator ('ode45' in MATLAB).

Furthermore, we have to solve the linear system of equations resulting from (6.1*c*) for $\psi^{(p)}_{,j}$, $j = 1\ldots N$, for given $\zeta_{,j}$ and $\varphi_{,j}$ at each time level. This is done by using a conjugate-gradient (CG) method, 'bicgstab' in MATLAB. Due to the use of Fourier series for determining derivatives, the associated system matrix is fully populated and evaluating the system of equations directly by matrix–vector multiplication will involve N^2 operations. Fortunately, at each stage in the CG method, not the system matrix, but only the vector of residuals for each of the equations is needed. This can efficiently be determined by use of the FFT, resulting in $N \log N$ operations, which is much less than N^2. The solution of the previous stage in the time-stepping procedure is used as an initial estimate for the solution $\psi^{(p)}_{,j}$, $j = 1\ldots N$.

The CG method is accelerated by using as a pre-conditioner the LU decomposition of a second-order central finite-difference approximation to (6.1*c*). As a result, only a few iterations (typically 2–7) are necessary to let the CG process converge to a relative residual norm of 10^{-7}. The overall computing time of the above described pseudo-spectral method is proportional to $N \log N$, i.e. almost proportional to N for large N.

Because the equations are nonlinear, the discretization may result in aliasing errors. The equations involve at most quartic operations on combinations of flow quantities (and depth h_0). If the flow quantities contain only energy for wavenumbers below k_{max}, the quartic operations will result in a transfer of energy to higher wavenumbers, up to $4\,k_{max}$. However, if this post-operation wavenumber is larger than the Nyquist wavenumber $k_N = \pi/\Delta x$, it will by aliasing fold back to the lower frequency $k_N - (4\,k_{max} - k_N)$. To prevent the contamination by aliasing of results for wavenumbers below k_{max}, we have to demand

$$k_{max} \leqslant k_N - 4\,k_{max}, \quad \text{which amounts to} \quad k_{max} \leqslant \frac{2}{5}k_N. \tag{6.3}$$

So, the time derivatives of $\zeta_{,j}$ and $\varphi_{,j}$, $j = 1\ldots N$, are spatially low-pass filtered to prevent aliasing by energy content in the wavenumber range above $2\pi/(5\Delta x)$.

No artificial damping or smoothing have been been used, apart from the small numerical damping inherent to the Runge–Kutta time integration used. The numerical model was found to be very robust, to which we think the positive-definiteness of the Hamiltonian density has contributed significantly.

T (s)	H (m)	kh_0	H/h_0
20†	3.0	0.1935	0.60
10	2.0	0.4367	0.40
6	1.8	0.8042	0.36
4	1.5	1.3872	0.30

† For the case $T = 20$ s and $H = 3.0$ m we have used 200 points per wavelength, instead of the 100 points per wavelength we have used in all other cases.

TABLE 1. Conditions for periodic waves over a horizontal bed.

Next, we will present several examples computed with the pseudo-spectral implementation of the parabolic structure model. First, periodic waves are considered, both over a horizontal bed and propagating over an underwater bar. Thereafter, the propagation of confined wave groups over a horizontal bed and a slope will be presented.

6.2. *Periodic waves*

6.2.1. *Periodic waves over a horizontal bed*

First, some test cases for periodic waves over a horizontal bed have been computed. As initial condition, we use accurate solutions according to fully nonlinear potential theory for periodic waves, computed with the method of Rienecker & Fenton (1981). In all cases we use a constant water depth $h_0 = 5$ m and $g = 9.81$ m s^{-2}. We consider the four wave conditions as given in table 1. The length of the periodic computational domain is equal to the wavelength.

The computed free-surface elevations after a simulation time of five wave periods are presented in figure 4. As can be seen, the model performs quite well. The phase speed of the nonlinear waves computed with the parabolic structure model is somewhat larger than the exact wave speed, in agreement with what has been found in the analysis of linear waves (see figure 1).

As an indication of the accuracy of the numerical method, we give the changes in the spatial-averaged values of the Hamiltonian and depth-integrated horizontal momentum (both divided by the fluid density), for the case of $T = 6$ s. The spatial-averaged Hamiltonian, i.e. sum of kinetic and potential energy per unit length, is initially equal to 3.684 m^3 s^{-2}, and reduces to -2.1×10^{-7} and -3.7×10^{-5} m^3 s^{-2} after, respectively, 5 and 1000 wave periods. The spatial-averaged horizontal momentum is initially equal to -2.1×10^{-8} m^2 s^{-1} (instead of zero, its exact value), and becomes -3.3×10^{-8} and -5.7×10^{-6} m^2 s^{-1} after 5 and 1000 wave periods respectively. These errors are mainly due to the errors in the CG solver for the elliptic equation and the numerical damping in the time-integration method. The spatial averages of the free-surface elevation ζ and potential gradient u are conserved to within machine accuracy.

6.2.2. *Periodic waves over an underwater bar*

As a second test case, we consider periodic waves propagating over an underwater bar (Dingemans 1997, § 5.9), for which measurements from a laboratory experiment are available (with the same experimental set-up as in Luth, Klopman & Kitou 1994). The experimental set-up is shown in figure 5(a), with the waves travelling from left to right. We will consider test case A, with waves of period $T = 2.857$ s and amplitude $a = 0.020$ m. The still water depth in front of the bar is 0.80 m, and on top of the bar 0.20 m. The front bed slope of the bar is 1/20, the 0.20 m depth region extends

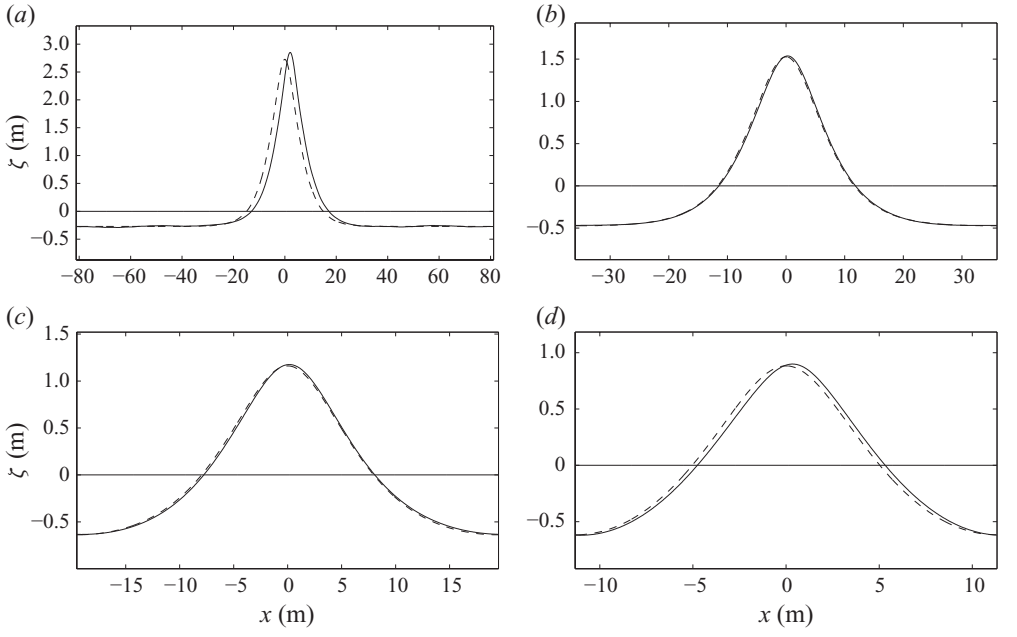

FIGURE 4. Snapshots of the free-surface elevation after five wave periods: the parabolic structure variational model (solid line) and the Rienecker and Fenton solution (Rienecker & Fenton 1981) (dashed line). $T = 20, 10, 6, 4$ s in (a), (b), (c), (d), respectively.

over 4.0 m and the back slope of the bar is 1/10. For further details we refer to Dingemans (1997) and Luth *et al.* (1994).

A snapshot of the computed free-surface elevation is shown in figure 5(b). As the waves propagate up the front slope, they increase in amplitude and are nonlinearly distorted. The generated superharmonics travel further as free waves after the shallow part of the bar. This generates a complex pattern of different frequency components travelling at different phase speeds after the bar. The amplitudes of free-surface harmonics at the carrier-wave frequency ω_0, as well as the amplitudes of the first three superharmonics, are shown in figure 5(c). As can be seen, the computed amplitudes compare quite well with the measured ones. Notice that the oscillations in the amplitude of the principal harmonic are due to (linear) reflections due to the bar bathymetry.

Since the parabolic structure model has the same linear dispersion characteristics as the model of Madsen *et al.* (1991), the results for the present parabolic structure model are very similar (see Dingemans 1997, figures 5.30–5.34). The phase speed of the free superharmonics after the bar, in relative deep water, is overestimated. This results in phase errors between the components, especially at furthest measuring locations 6 and 12. Models with better linear dispersion characteristics are known to perform better in this region (see e.g. Dingemans 1994; Dingemans 1997, § 5.9.3; Lynett & Liu 2004*a*). In the present approach, this may be achieved by using for instance the cosh structure model with well-chosen x-variations of the parameter κ (see figure 1), or the general series model with $M \geqslant 3$ (see figure 2).

6.3. *Confined wave groups*

When wave groups propagate over variable bathymetry, one has besides the distortion of the wave group (Djordjević & Redekopp 1978; Turpin, Benmoussa & Mei 1983)

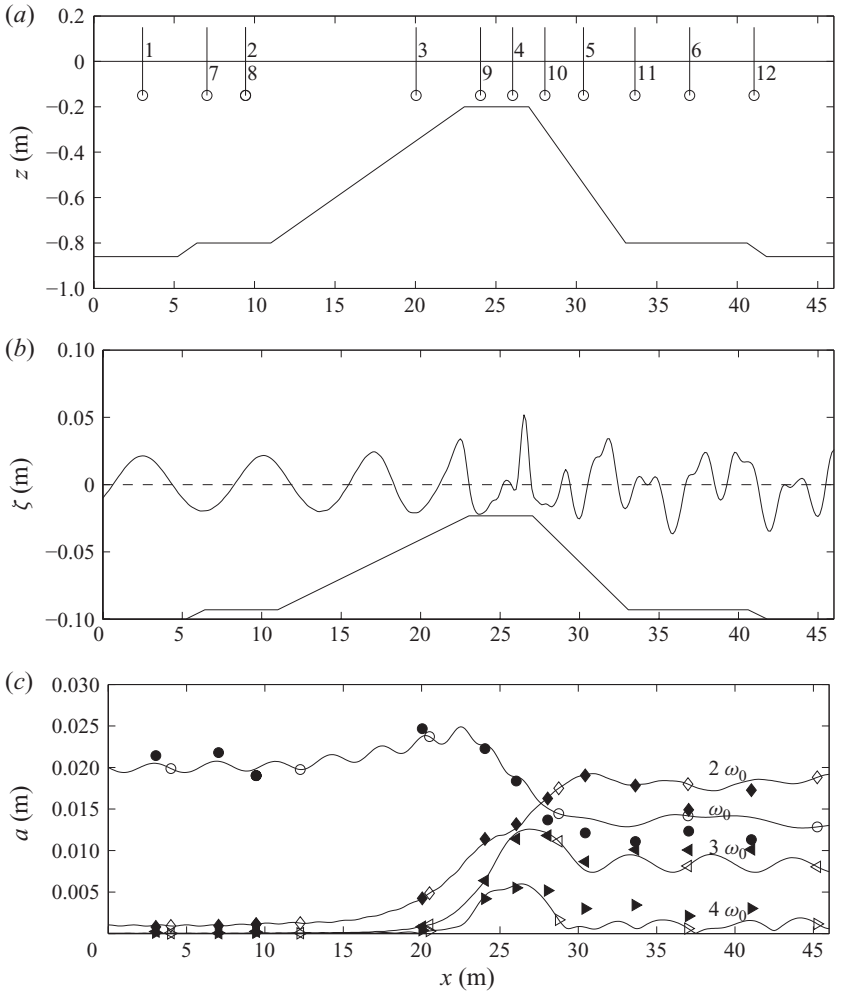

FIGURE 5. Periodic waves over a bar, test case A. (*a*) Experimental set-up, showing bottom topography and measurement locations 1–12. (*b*) Snapshot of the computed free-surface elevation at $t = 60$ s, and bottom topography (on a different, vertical distorted scale). (*c*) Amplitudes of surface elevation harmonics as a function of x, for the computation (open symbols and lines) and measurements (filled symbols), at the carrier-wave frequency ω_0 ($\bigcirc$), and superharmonic frequencies $2\,\omega_0$ ($\diamond$), $3\,\omega_0$ ($\triangleleft$) and $4\,\omega_0$ ($\triangleright$).

also the effect of the generation of free long waves (Mei & Benmoussa 1984; Liu 1989). These long waves are of interest for coastal morphology and the forcing of moored floating structures and ships. Here, we will study the capabilities of the variational Boussinesq model with parabolic vertical structure in predicting wave group deformation and long wave generation. This will be done using confined wave groups, with a sech (hyperbolic-secant) envelope of the carrier waves.

First, we will look into the propagation of a confined wave group over a horizontal bed, and look into its deformation as it propagates and the emission of spurious waves due to imperfect initial conditions. Second, the propagation of this wave group over a slope into a shallower constant-depth region will be computed, and compared with the results of van Groesen & Westhuis (2002).

The initial water depth in all computations is $h_0 = 12$ m, the carrier-wave frequency of the confined wave group is $\omega_0 = \pi/3$ rad s^{-1}, the carrier-wave amplitude in the centre of the group is $a_0 = 1.0$ m and the gravitational acceleration is $g = 9.81$ m s^{-2}. The spatial step was taken equal to 2 m in all subsequent computations, i.e. about 25 points per wavelength. With the maximum wavenumber restricted by (6.3), this means that up to the fifth spatial harmonic can be represented on this grid.

The initial conditions for the free-surface elevation $\zeta(x, t)$ and potential-gradient $u(x, t)$, including second-order subharmonics and superharmonics, as well as second-order modulation effects on $u(x, t)$, were computed from the formulations as given in Dingemans & Otta (2001, equations (39)–(45), (101)–(103)). These initial conditions correspond with the hyperbolic-secant solution of the nonlinear Schrödinger (NLS) equation, as derived by a multiple-scales perturbation-series approach from the full nonlinear potential flow problem. An NLS equation derived from the parabolic structure model will have slightly different values of the coefficients and the second-order subharmonics and superharmonics. Notice that there is a small typographical error in (44) of Dingemans & Otta (2001): the second transformation should be $\kappa_2^{\phi} = (\omega^2/g^2)\kappa_2^{\zeta}$.

6.3.1. *Confined wave group over a horizontal bed*

Given the initial conditions for ζ and u as specified above, the flow evolution equations are computed for 900 s, i.e. 150 carrier-wave periods. The results are shown in figure 6. As can be seen, the wave group envelope does not deform much, after travelling for about 100 carrier wavelengths and five wave-group lengths. The wave envelope has become a bit narrower and peaked, and slightly asymmetrical horizontally around its centre.

Further, some spurious waves are shed, by the deviation of the parabolic structure model from the fully nonlinear potential-flow equations, as well as from the approximations underlying the NLS equation. In figure 6(*c*) a spurious wave group with wavenumber $2k_0$ twice the carrier wavenumber k_0 is seen, of amplitude 0.01 m, i.e. about 1 % of the carrier-wave amplitude $a_0 = 1.0$ m. These spurious waves travel slower than the carrier waves. In figure 6(*d*) a near-solitary long wave of about 2.5 mm height has travelled about twice the distance of the carrier-wave group. Finally, in figure 6(*e*) a group of left-travelling spurious waves with wavenumbers near $2k_0$ and higher can be found, of amplitudes less than 2 mm.

6.3.2. *Confined wave group on a slope*

Next, we will consider the same confined wave group encountering an underwater slope. Significant depth changes will start at shorter distances from the initial wave group location than the group travel distance discussed above. Therefore, we may consider the previously discussed initial wave conditions an adequate approximation to the 'exact' soliton-envelope wave-group solution to the parabolic structure model (if it exists).

The confined wave group will now propagate from a region with initial and constant water depth $h_0 = 12$ m, via a 0.012 slope of 500 m horizontal extent, into another region of constant and shallower depth, $h_0 = 6$ m. We will compare our results with those of van Groesen & Westhuis (2002) (see also Westhuis 2001), who use a finite element method to solve the fully nonlinear problem of surface waves on a potential flow. Van Groesen & Westhuis (2002) use a different method to initialize the

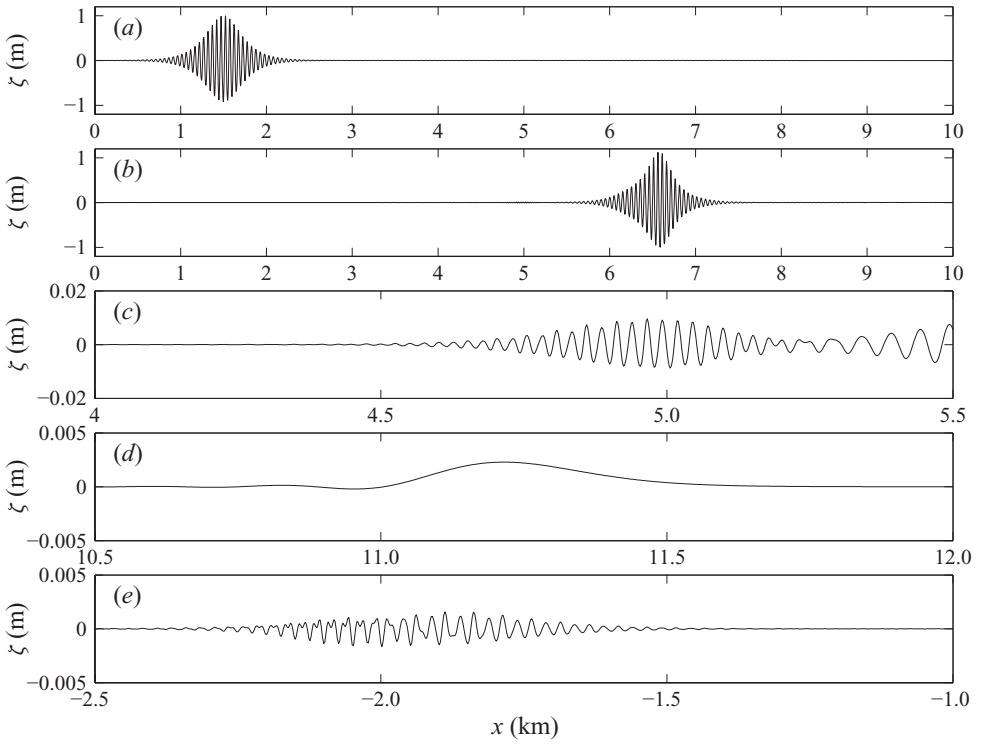

FIGURE 6. Surface elevation for a confined wave group over a horizontal bed and scattered spurious waves. (*a*) Wave group at $t = 0$ s, (*b*) wave group at $t = 900$ s, (*c*) detail of slow right-travelling short-wave tail at $t = 900$ s, (*d*) detail of fast right-travelling long wave at $t = 900$ s, (*e*) detail of slow left-travelling short-wave group at $t = 900$ s.

confined wave group. This, in itself, will create some differences between their and our results.

Notice that in the deeper part we have for the carrier waves a relative depth $k_0 h_0 = 1.49$, and in the shallow part $k_0 h_0 = 0.92$. At $kh = 1.36$ the nonlinearity coefficient in the NLS equation changes sign (see e.g. Benjamin & Feir 1967). So, for the NLS equation, we go from the focusing regime for $kh > 1.36$ in the deeper part, where the hyperbolic-secant soliton solution exists, to the defocusing regime with $kh < 1.36$.

Two snapshots of the free surface elevation at $t = 0$ and 900 s, as computed with the parabolic structure model, are given in figure 7. Clearly the deformation of the wave group, as well as the generation of a free long wave, can be seen. In order to compare with van Groesen & Westhuis (2002), some details are given in figure 8 at $t = 900$ s. Note the appearance of the longer waves in the front of the deforming wave group and the shorter waves in its tail. There is quite good agreement, both in the evolution of the carrier-wave amplitude (figure 8*a*) as well as in the generated free long wave (figure 8*b*). However, there are phase differences between the two models, which we address now. In figure 8 the phase difference is small near the front of the wave group at $x = 7$ km, and the phase difference is about half a wavelength in error near $x = 6$ km. With a carrier wavelength of about 41 m this is a localization error of approximately 20 m over a wave group length of $\approx$25 waves, and after propagating over more than a hundred carrier wavelengths.

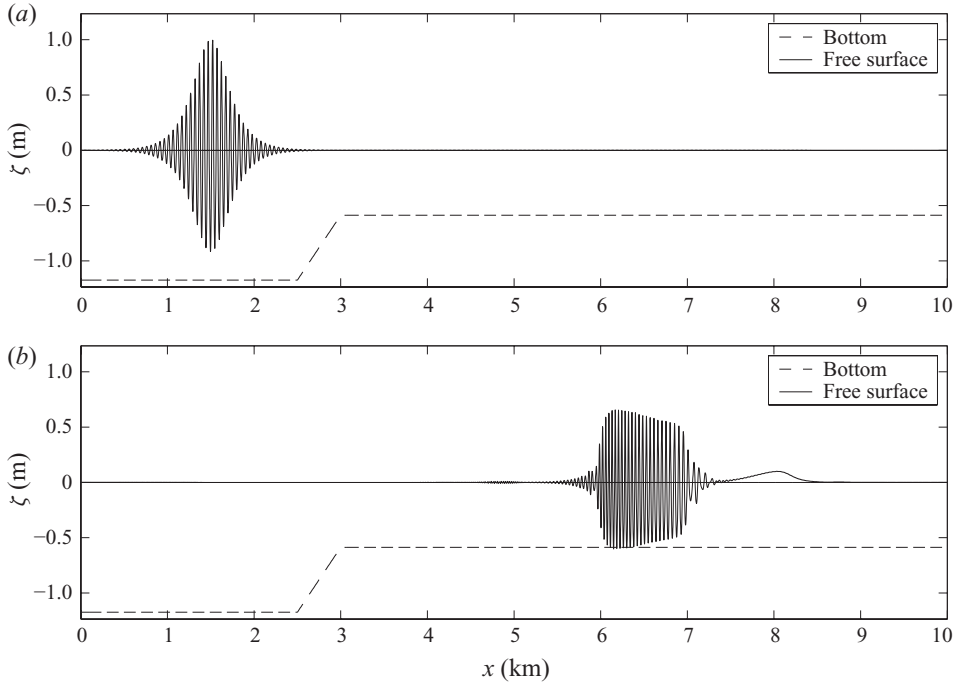

FIGURE 7. Wave group propagating over a slope: surface elevation $\zeta(x,t)$ (solid line) as a function of x. (*a*) $t=0$ s, and (*b*) $t=900$ s. The dashed line is the bottom elevation (not to scale).

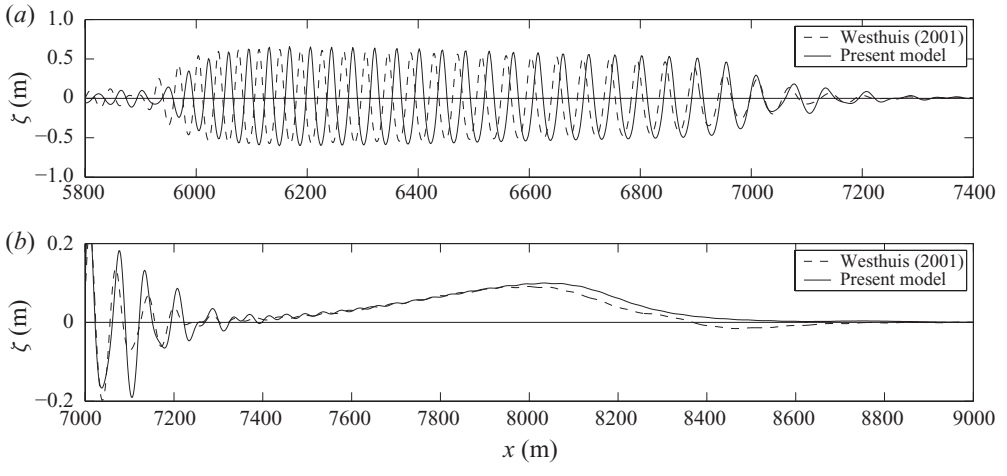

FIGURE 8. Wave group propagating over a slope: details of the surface elevation $\zeta(x,t)$ as a function of x at $t=900$ s. Present parabolic structure model (solid line) and the model of van Groesen & Westhuis (2002) (dashed line).

Analysis showed us that the observed phase differences cannot be explained by either the phase-speed error introduced by the model approximation or the one from the numerical method. We conclude that the difference is due to the difference in the initial conditions used in our model compared to those used by Westhuis (2001) (see figure 9). As can be observed, differences appear at the front of the wave group

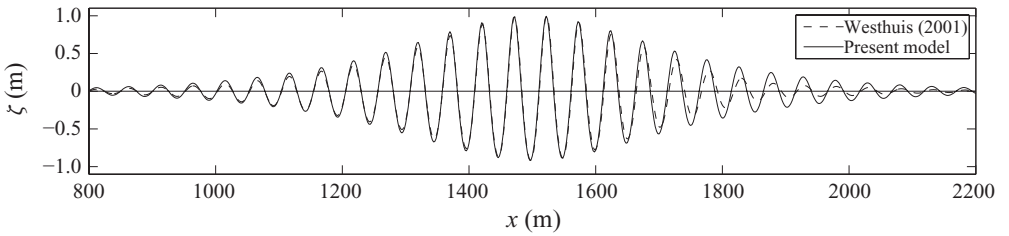

FIGURE 9. Wave group propagating over a slope: initial condition of the surface elevation $\zeta(x,t)$ as a function of x at $t=0$ s. Present parabolic structure model (solid line) and the model of van Groesen & Westhuis (2002) (dashed line).

($x > 1500$ m). In this region, the wave amplitudes by Westhuis (2001) are smaller than the theoretical ones.

7. Conclusions

Variational Boussinesq models with positive-definite Hamiltonian density, i.e. energy densities per unit of horizontal area, are presented. The models are derived by approximating the horizontal and vertical velocities in the kinetic energy, using a series expansion with a small number of vertical shape functions for the velocity (potential).

It is essential that the first shape function equals one at the free surface and all other shape functions are zero at the free surface. This ensures that only two time-evolution equations appear in terms of the canonical variables, viz. the surface elevation $\zeta(\boldsymbol{x},t)$ and the free-surface potential $\varphi(\boldsymbol{x},t)$ in the case of a velocity potential model (see (4.3*a*,*b*)). The additional parameters $\psi_m(\boldsymbol{x},t)$ are solved by a (series of) second-order elliptic equations, linear in $\psi_m(\boldsymbol{x},t)$ (see (4.3*c*)). All equations contain only low-order partial derivatives: first-order time derivatives, second-order spatial derivatives for the Hamiltonian models written in the surface potential and third-order spatial derivatives for the models written in terms of velocities. No mixed space–time derivatives appear. The cost is, as compared to classical Boussinesq models, that we have to solve (a series of) additional elliptic equations in the flow parameters $\psi_m(\boldsymbol{x},t)$ associated with the introduced shape function(s).

The variational Boussinesq models thus derived have a positive-definite Hamiltonian, which is important for a good dynamical behaviour of the model. Further, several symmetries of the 'exact' Hamiltonian for water waves are also transferred to the variational Boussinesq models. This results in associated conservation laws, among others depth-integrated mass conservation and energy conservation (for a horizontal bed also momentum conservation). Apart from the approximations to the vertical velocity structure (which may include a non-essential mild-slope approximation), no further approximations are made. The resulting models are therefore fully nonlinear, i.e. without approximations regarding the wave amplitude.

As examples, we have derived vertical flow structure models with one parabolic shape function, one hyperbolic-cosine shape function and a polynomial power-series expansion with several parameters. The linear characteristics of these models are studied, using the average Lagrangian. The resulting linear frequency-dispersion relationships are all well behaved, i.e. no real-valued poles in the resulting rational functions in terms of the wavenumber k. This is a result of the positive-definite

Hamiltonian. Also, wave action conservation can be used to show the integral effect of linear shoaling from one location with a certain depth (and group velocity) to another.

To study the nonlinear characteristics, we present numerical simulations for the parabolic structure model in one horizontal dimension, using a pseudo-spectral method. We only worked out numerical results for the parabolic structure model, because it is the simplest of the models considered. We expect that the cosh structure model and the power-series structure model (with $M > 2$) are able to give more accurate results. For practical purposes, we recommend using the cosh structure model, since it provides a good balance between accuracy on arbitrary depth and numerical efforts. However, this is a point for further study. Recently, it has been shown by Dingemans & Klopman (2009) that reflection properties are much improved by a different normalization of the structure functions. Further properties are still under investigation.

Using the parabolic structure model, the propagation and deformation of periodic waves and confined wave groups have been computed, both over a horizontal bed and over bathymetry. Comparison with other numerical methods, solving the fully nonlinear potential-flow problem, as well as with measurements, show the capabilities of the model. Besides, no numerical instabilities have been encountered, despite the absence of dissipation in the numerical model – apart from the small dissipation in the Runge–Kutta time integration. This may be attributed to the positive-definiteness of the Hamiltonian density.

Appendix. Vertical integrals for the parabolic, cosh and power-series structure model

For the parabolic vertical structure of the flow, as given by (3.1), the integrals (4.2) and their ζ-derivatives become, using as before $h \equiv h_0 + \zeta$ and dropping the indices (since $M = 1$):

$$F^{(p)} = \frac{2}{15}h^3, \quad F'^{(p)} = \frac{2}{5}h^2, \quad G^{(p)} = \frac{7}{15}h, \quad G'^{(p)} = \frac{7}{15}, \tag{A 1a}$$

$$K^{(p)} = \frac{1}{3}h, \quad K'^{(p)} = \frac{1}{3}, \quad P^{(p)} = -\frac{1}{3}h^2, \quad P'^{(p)} = -\frac{2}{3}h, \tag{A 1b}$$

$$Q^{(p)} = -\frac{2}{3}h, \quad Q'^{(p)} = -\frac{2}{3}, \quad R^{(p)} = \frac{1}{5}h^2, \quad R'^{(p)} = \frac{2}{5}h. \tag{A 1c}$$

Under the hyperbolic-cosine assumption for the vertical flow structure, as given in (4.6), the integrals from (4.2) become

$$F^{(c)} = -\frac{3}{2}\frac{1}{\kappa}\mathscr{S}\mathscr{C} + \frac{1}{2}h + h\mathscr{C}^2, \quad F'^{(c)} = 2\kappa h\mathscr{S}\mathscr{D}, \tag{A 2a}$$

$$G^{(c)} = \kappa^2 h\mathscr{S}^2, \quad G'^{(c)} = \kappa^2\mathscr{S}[2\kappa h\mathscr{C} + \mathscr{S}], \tag{A 2b}$$

$$K^{(c)} = \frac{1}{2}\kappa\mathscr{S}\mathscr{C} - \frac{1}{2}\kappa^2 h, \quad K'^{(c)} = \kappa^2\mathscr{S}^2, \tag{A 2c}$$

$$P^{(c)} = -h\mathscr{D}, \quad P'^{(c)} = -\kappa h\mathscr{S}, \tag{A 2d}$$

$$Q^{(c)} = -\kappa h\mathscr{S}, \quad Q'^{(c)} = -\kappa^2 h\mathscr{C} - \kappa\mathscr{S}, \tag{A 2e}$$

$$R^{(c)} = \kappa h\mathscr{S}\mathscr{D}, \quad R'^{(c)} = \kappa^2 h[\mathscr{C}^2 + \mathscr{S}^2] - \kappa\mathscr{S}\mathscr{C} \tag{A 2f}$$

with

$$\mathscr{D} \equiv \cosh(\kappa h) - \frac{\sinh(\kappa h)}{\kappa h}, \quad \mathscr{S} \equiv \sinh(\kappa h) \quad \text{and} \quad \mathscr{C} \equiv \cosh(\kappa h). \tag{A 3}$$

For the power-series flow structure, as given in (4.11), the integrals and their derivatives become

$$F^{(s)}_{mn} = (-1)^{m+n} \frac{h^{m+n+1}}{m+n+1}, \quad F'^{(s)}_{mn} = (-1)^{m+n} h^{m+n}, \tag{A 4a}$$

$$G^{(s)}_{mn} = (-1)^{m+n} mn \frac{h^{m+n-1}}{m+n-1}, \quad G'^{(s)}_{mn} = (-1)^{m+n} mn h^{m+n-2}, \tag{A 4b}$$

$$K^{(s)}_{mn} = G^{(s)}_{mn}, \quad K'^{(s)}_{mn} = G'^{(s)}_{mn}, \tag{A 4c}$$

$$P^{(s)}_{m} = (-1)^{m} \frac{h^{m+1}}{m+1}, \quad P'^{(s)}_{m} = (-1)^{m} h^{m}, \tag{A 4d}$$

$$Q^{(s)}_{m} = (-1)^{m-1} h^{m}, \quad Q'^{(s)}_{m} = (-1)^{m-1} m h^{m-1}, \tag{A 4e}$$

$$R^{(s)}_{mn} = (-1)^{m+n-1} n \frac{h^{m+n}}{m+n}, \quad R'^{(s)}_{mn} = (-1)^{m+n-1} n h^{m+n-1}. \tag{A 4f}$$

REFERENCES

Agnon, Y., Madsen, P. A. & Schäffer, H. A. 1999 A new approach to high-order Boussinesq models. *J. Fluid Mech.* **399**, 319–333.

Benjamin, T. B. 1984 Impulse, flow force and variational principles. *IMA J. Appl. Math.* **32** (1–3), 3–68 (with errata in the preamble of the same issue).

Benjamin, T. B. & Feir, J. E. 1967 The disintegration of wave trains on deep water. Part 1. Theory. *J. Fluid Mech.* **27** (3), 417–430.

Benjamin, T. B. & Olver, P. J. 1982 Hamiltonian structure, symmetries and conservation laws for water waves. *J. Fluid Mech.* **125**, 137–185.

Boussinesq, J. 1872 Théorie des ondes et des remous qui se propagent le long d'un canal rectangulaire horizontal, en communiquant au liquide contenu dans ce canal des vitesses sensiblement pareilles de la surface au fond. *J. Math. Pure. Appl.,* Deuxième Sér. **17**, 55–108.

Bretherton, F. P. 1968 Propagation in slowly varying waveguides. *Proc. R. Soc. Lond.* A **302** (1471), 555–576.

Brizard, A. J. 2005 Noether methods for fluids and plasmas. *J. Plasma Phys.* **71** (2), 225–236.

Broer, L. J. F. 1974 On the Hamiltonian theory of surface waves. *Appl. Sci. Res.* **29**, 430–446.

Broer, L. J. F. 1975 Approximate equations for long wave equations. *Appl. Sci. Res.* **31** (5), 377–395.

Broer, L. J. F., van Groesen, E. W. C. & Timmers, J. M. W. 1976 Stable model equations for long water waves. *Appl. Sci. Res.* **32** (6), 619–636.

Chen, Y. & Liu, P. L.-F. 1995 Modified Boussinesq equations and associated parabolic models for water wave propagation. *J. Fluid Mech.* **288**, 351–381.

Dingemans, M. W. 1994 *Comparison of Computations With Boussinesq-Like Models and Laboratory Measurements*. MAST-G8M note, H1684. Delft Hydraulics, 32 pp.

Dingemans, M. W. 1997 *Water Wave Propagation Over Uneven Bottoms*. Advanced Series on Ocean Engineering, vol. 13. World Scientific, 2 Parts, 967 pp.

Dingemans, M. W. & Klopman, G. 2009 Effects of normalization and mild-slope approximation on wave reflection by bathymetry in a Hamiltonian wave model. In *Proceedings of Twenty-Fourth International Workshop on Water Waves and Floating Bodies,* Zelenogorsk, Russia.

Dingemans, M. W. & Otta, A. K. 2001 Nonlinear modulation of water waves. In *Advances in Coastal and Ocean Engineering* (ed. P. L.-F. Liu), vol. 7, pp. 1–76. World Scientific.

Djordjević, V. D. & Redekopp, L. G. 1978 On the development of packets of surface gravity waves moving over an uneven bottom. *J. Appl. Math. Phys. (ZAMP)* **29**, 950–962.

Dommermuth, D. G. & Yue, D. K. P. 1987 A high-order spectral method for the study of nonlinear gravity waves. *J. Fluid Mech.* **184**, 267–288.

Fuhrman, D. R. & Bingham, H. B. 2004 Numerical solutions of fully nonlinear and highly dispersive Boussinesq equations in two horizontal dimensions. *Intl J. Numer. Methods Fluids* **44** (3), 231–255.

van Groesen, E. & Westhuis, J. H. 2002 Modelling and simulation of surface water waves. *Math. Comput. Sim.* **59** (4), 341–360.

Hayes, W. D. 1970*a* Conservation of action and modal wave action. *Proc. R. Soc. Lond.* A **330** (1541), 187–208.

Hayes, W. D. 1970*b* Kinematic wave theory. *Proc. R. Soc. Lond.* A **330** (1541), 209–226.

Hayes, W. D. 1973 Group velocity and nonlinear dispersive wave propagation. *Proc. R. Soc. Lond.* A **332** (1589), 199–221.

Hsiao, S.-C., Lynett, P., Hwung, H.-H. & Liu, P. L.-F. 2005 Numerical simulations of nonlinear short waves using a multilayer model. *J. Engng Mech.* **131** (3), 231–243.

Katopodes, N. D. & Dingemans, M. W. 1989 Hamiltonian approach to surface wave models. In *Computational Modelling and Experimental Methods in Hydraulics (HYDROCOMP '89),* Dubrovnik, Yugoslavia (ed. Č. Maksimovič & M. Radojkovič), pp. 137–147. Elsevier.

Klopman, G., Dingemans, M. W. & van Groesen, E. 2005 A variational model for fully nonlinear water waves of Boussinesq type. In *Proceedigs of Twentieth International Workshop on Water Waves and Floating Bodies,* Longyearbyen, Spitsbergen, Norway.

Liu, P. L.-F. 1989 A note on long waves induced by short-wave groups over a shelf. *J. Fluid Mech.* **205**, 163–170.

Ludwig, D. 1970 Modified W.K.B. method for coupled ionospheric equations. *J. Atmos. Terr. Phys.* **32** (6), 991–998.

Luth, H. R., Klopman, G. & Kitou, N. 1994 Project 13g: kinematics of waves breaking partially on an offshore bar. LDV measurements for waves with and without a net onshore current. *Tech. Rep.* H1573. Delft Hydraulics, Delft, The Netherlands, 40 pp.

Lynett, P. J. & Liu, P. L.-F. 2004*a* A two-layer approach to wave modelling. *Proc. R. Soc. Lond.* A **460** (2049), 2637–2669.

Lynett, P. J. & Liu, P. L.-F. 2004*b* Linear analysis of the multi-layer model. *Coast. Engng* **51** (5–6), 439–454.

Madsen, P. A., Bingham, H. B. & Schäffer, H. A. 2003 Boussinesq-type formulations for fully nonlinear and extremely dispersive water waves: derivation and analysis. *Proc. R. Soc. Lond.* A **459**, 1075–1104.

Madsen, P. A., Murray, R. & Sørensen, O. R. 1991 A new form of the Boussinesq equations with improved linear dispersion characteristics. *Coast. Engng* **15** (4), 371–388.

Madsen, P. A. & Sørensen, O. R. 1992 A new form of the Boussinesq equations with improved linear dispersion characteristics. Part 2. A slowly-varying bathymetry. *Coast. Engng* **18** (3–4), 183–204.

Mei, C. C. & Benmoussa, C. 1984 Long waves induced by short-wave groups over an uneven bottom. *J. Fluid Mech.* **139**, 219–235.

Milder, D. M. 1977 A note on: 'On Hamilton's principle for surface waves'. *J. Fluid Mech.* **83** (1), 159–161.

Milder, D. M. 1990 The effect of truncation on surface-wave Hamiltonians. *J. Fluid Mech.* **216**, 249–262.

Miles, J. W. 1977 On Hamilton's principle for surface waves. *J. Fluid Mech.* **83** (1), 153–158.

Otta, A. K., Dingemans, M. W. & Radder, A. C. 1996 A Hamiltonian model for nonlinear water waves and its applications. In *Proceedings of 25th International Conference Coastal Engineering,* Orlando, vol. 1, pp. 1156–1167. ASCE, New York.

Radder, A. C. 1992 An explicit Hamiltonian formulation of surface waves in water of finite depth. *J. Fluid Mech.* **237**, 435–455.

Radder, A. C. 1999 Hamiltonian dynamics of water waves. In *Advance in Coastal and Ocean Engineering* (ed. P. L.-F. Liu), vol. 4, pp. 21–59. World Scientific.

Rienecker, M. M. & Fenton, J. D. 1981 A Fourier approximation method for steady water waves. *J. Fluid Mech.* **104**, 119–137.

Shepherd, T. G. 1990 Symmetries, conservation laws, and Hamiltonian structure in geophysical fluid dynamics. *Adv. Geophys.* **32**, 287–338.

Turpin, F.-M., Benmoussa, C. & Mei, C. C. 1983 Effects of slowly varying depth and current on the evolution of a Stokes wavepacket. *J. Fluid Mech.* **132**, 1–23.

West, B. J., Brueckner, K. A., Janda, R. S., Milder, D. M. & Milton, R. L. 1987 A new numerical method for surface hydrodynamics. *J. Geophys. Res.* **92** (C11), 11803–11824.

Westhuis, J.-H. 2001 The numerical simulation of nonlinear waves in a hydrodynamic model test basin. PhD thesis, University of Twente, Enschede, The Netherlands.

Whitham, G. B. 1967 Variational methods and applications to water waves. *Proc. R. Soc. Lond.* A **299** (1456), 6–25.

Whitham, G. B. 1974 *Linear and Nonlinear Waves*. Wiley Interscience.

Witting, J. M. 1984 A unified model for the evolution of nonlinear water waves. *J. Comput. Phys.* **56** (4), 203–236.

Zakharov, V. E. 1968 Stability of periodic waves of finite amplitude on the surface of a deep fluid. *J. Appl. Mech. Technol. Phys.* **9** (2), 190–194 (originally published in *Z. Prildadnoi Mekh. Tekh. Fiz.* **9** (2), pp. 86–94, 1968).